

Series Editor
Gilles Pijaudier-Cabot

Numerical Simulation, An Art of Prediction 2

Examples

Jean-François Sigrist

Color section

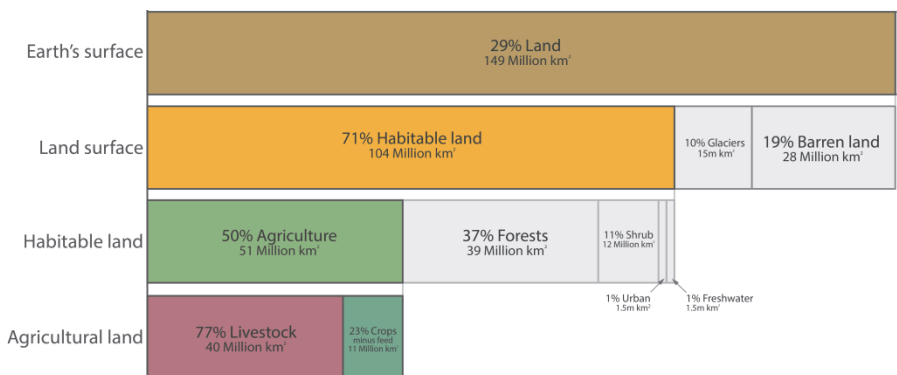


Figure 1.2. Allocation of land areas for food production (source: Our World in Data/<https://ourworldindata.org/yields-and-land-use-in-agriculture>)

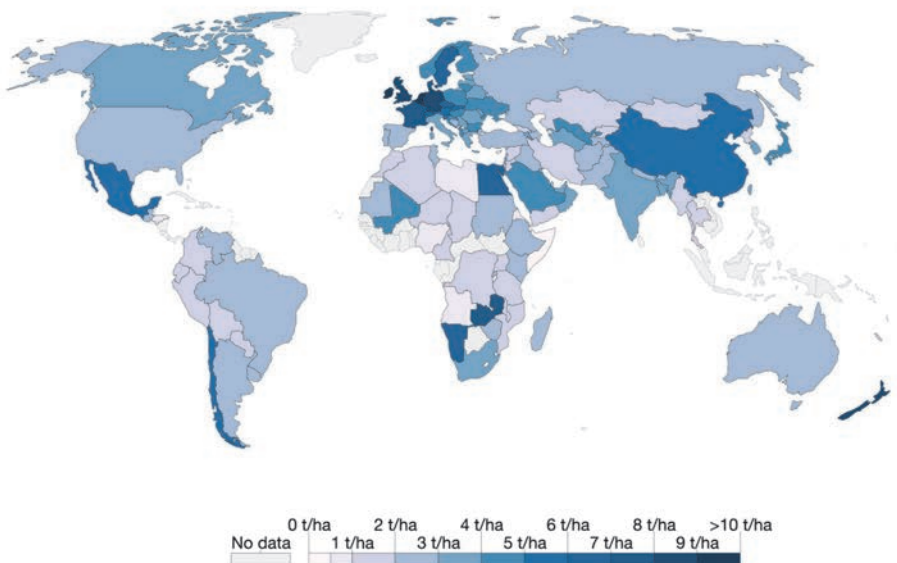


Figure 1.4. Annual world wheat yields for 2014, expressed in tons per hectare. Wheat is the primary cereal produced in the world, aimed at both human and animal consumption (source: Our World in Data/<https://ourworldindata.org/yields-and-land-use-in-agriculture>)



Figure 1.5. Although edible, these tomatoes, produced in France, are discarded because they do not meet certain criteria based on the standardization of production and their packaging (source: © Jacques Péré, from the series “La Beauté du diable”, exhibition at the Galerie Lyeux Communs, Tours, June 2018)

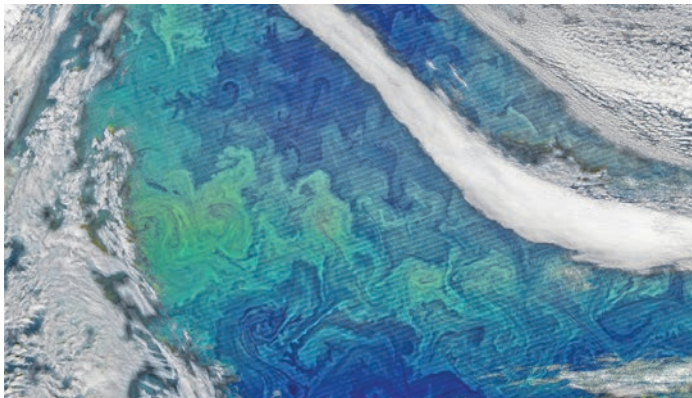


Figure 1.7. Satellite image showing algae growth in a North Atlantic region (source: www.nasa.gov)

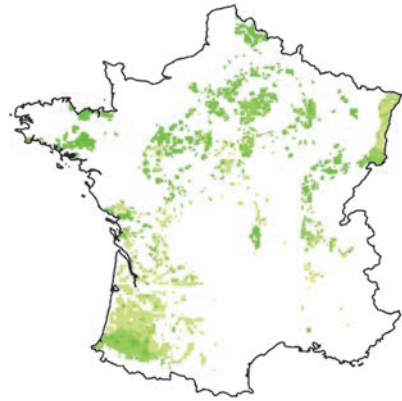
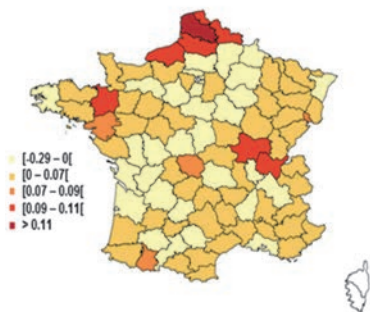


Figure 1.10. Share of production allowed by the ecosystem services associated with grain maize cultivation [THE 17]



Figure 1.11. Working hours (per ha and per year) required by a farmer for “conventional” agricultural production (yellow squares) and pesticide-free production (orange triangles), as part of a durum wheat and sunflower crop rotation, in southwest France [RAY 17]

A



B

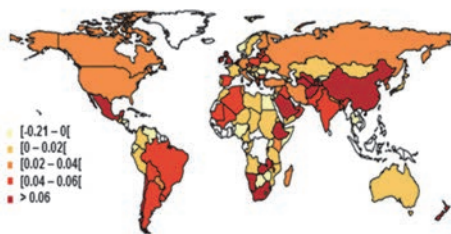


Figure 1.13. Calculation of wheat crop yields in France and worldwide: the figure represents yield increases estimated by statistical methods, in different countries of the world and for the French departments. The unit is the ton of wheat per hectare cultivated and per year [MIC 13]

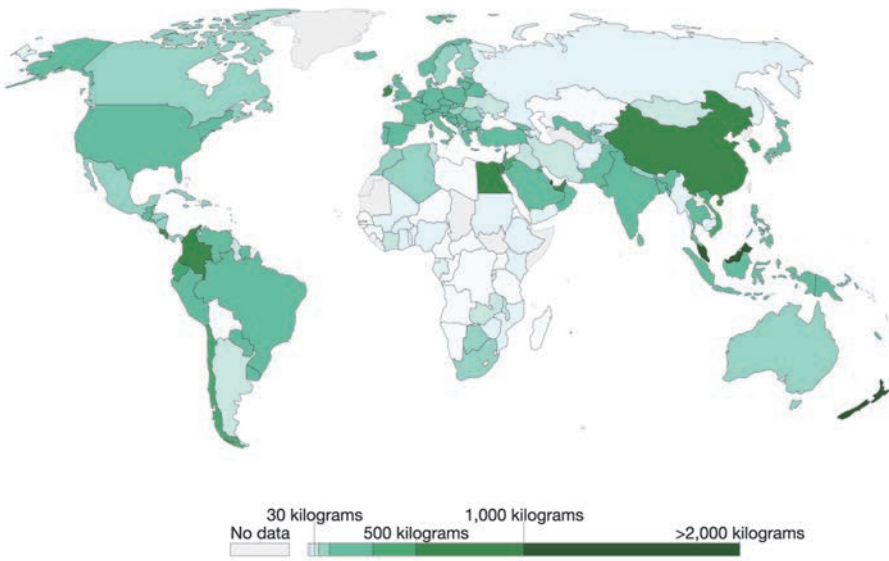


Figure 1.15. Global use of nitrogen, potassium and phosphate fertilizers worldwide in 2014: major agricultural countries are making massive use of fertilizers. The quantities used are expressed in kilograms per hectare of cultivated land (source: Our World in Data/<https://ourworldindata.org/fertilizer-and-pesticides>)

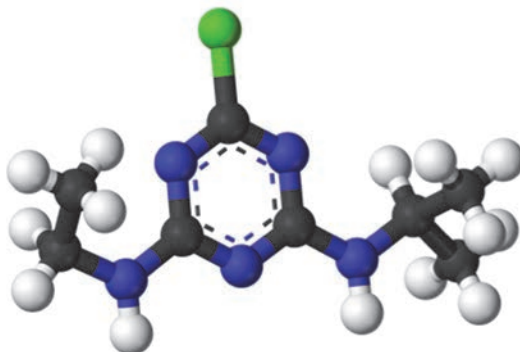


Figure 1.17. 3D representation of atrazine (source: www.commonswikimedia.org). For a color version of this figure, see www.iste.co.uk/sigrist/simulation2.zip

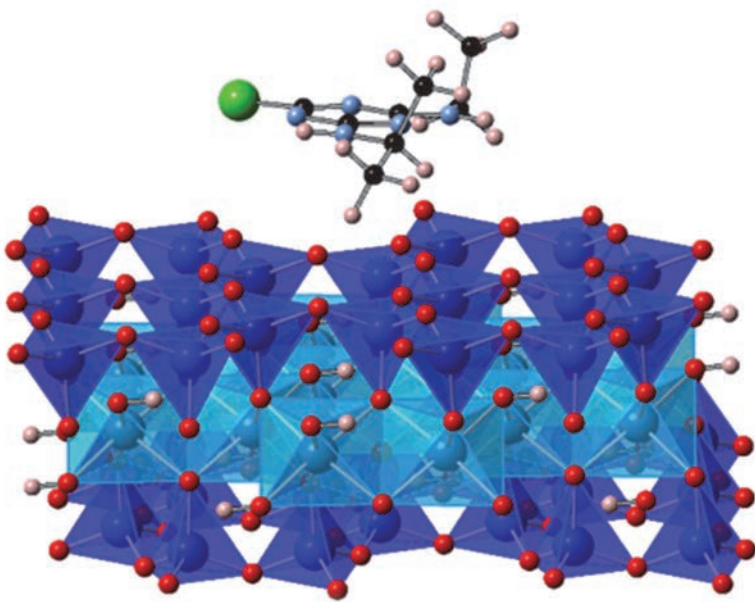


Figure 1.18. Example of calculation at the atomic scale [BEL 17b]. For a color version of this figure, see www.iste.co.uk/sigrist/simulation2.zip



Figure 1.19. Vegetation map obtained from satellite observations
(source: NASA/www.nasa.gouv)



Figure 2.1. To which countries does the world export? (source: Observatory for Economic Complexity/www.atlas.media.mit.edu)



(a) Maritime traffic (source: www.shipmap.org)



(b) Air traffic (source: www.theguardian.com)

Figure 2.3. Visualization of maritime and air traffic

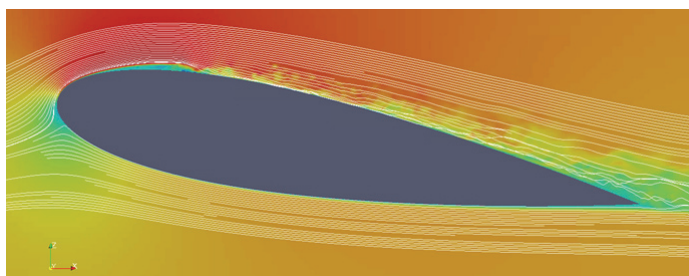


Figure 2.4. Flow calculation around a lifting profile (source: Naval Group)

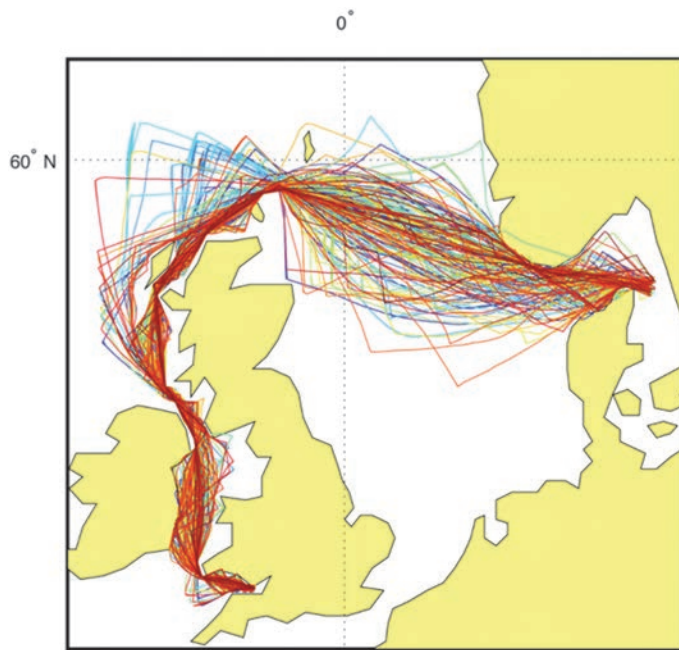


Figure 2.6. Simulation of possible routes for an offshore race (image made using Neptune code, routing software developed by Xavier Pillons; source: BMD/www. www.bmuyt.com)

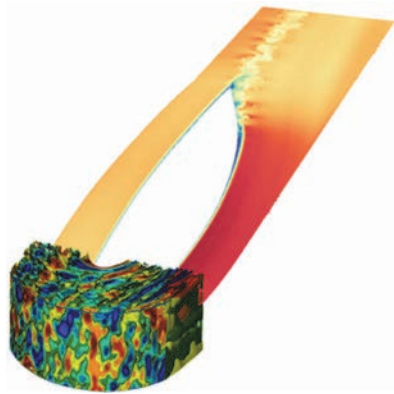
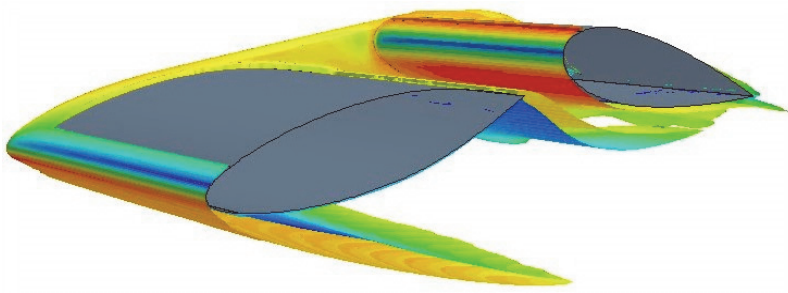
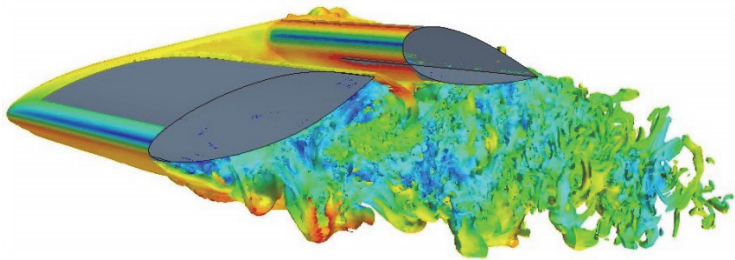


Figure 2.12. Flow calculation around a bearing profile with turbulence resolution



(a) Calculation with average modeling



(b) Calculation with resolution of large scales

Figure 2.13. Examples of hydrodynamic calculations around a hull appendage (source: Sirehna/Naval Group)

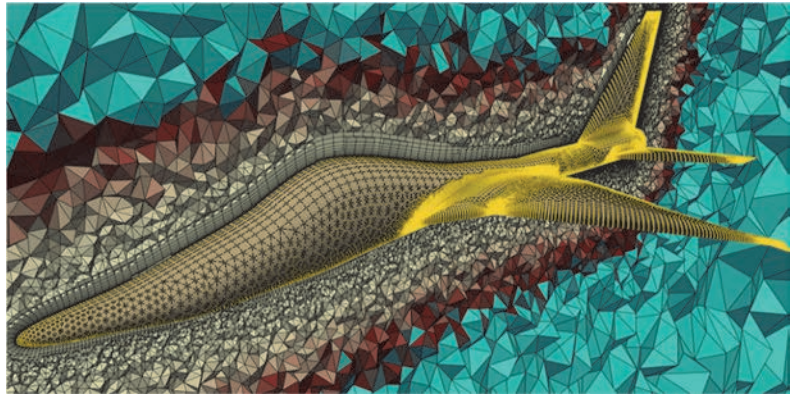


Figure 2.14. Meshing of the fluid in finite volumes around an aircraft (source: www.blog.pointwise.com)

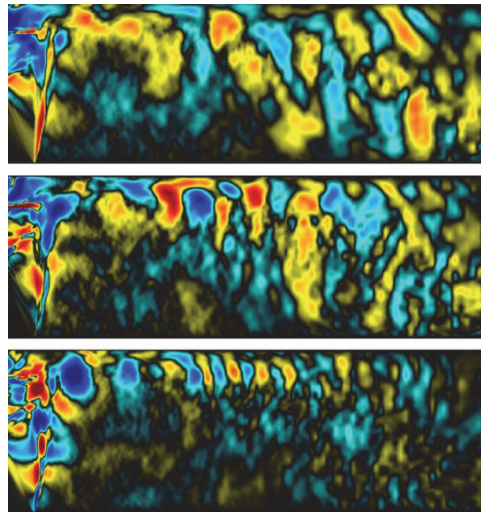
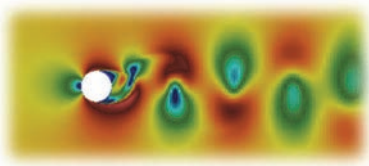
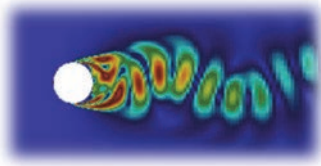


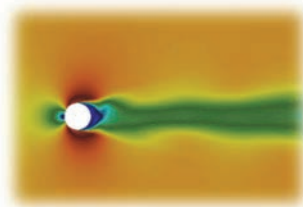
Figure 2.15. Modal analysis of a flow [KAR 18]



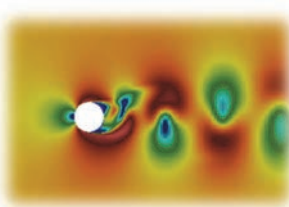
(a) Complete flow calculation



(b) A mode of flow



(c) Calculation with a mode



(d) Calculation with five modes

Figure 2.16. Calculation of water flow downstream of a cylinder with a reduced order model

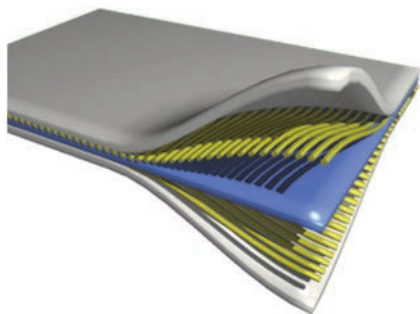
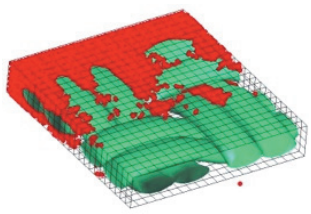
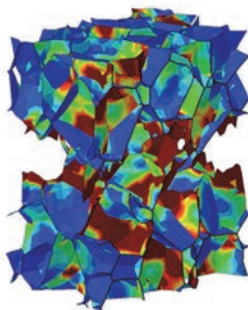


Figure 2.18. Example of a composite material: a multilayer (source: www.commons.wikimedia.org)

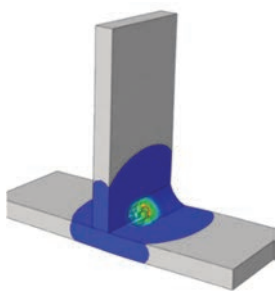


(a) Resin injection simulation
[COM 05]

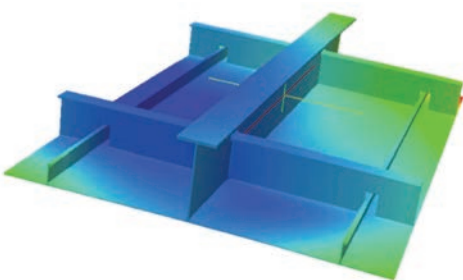


(b) Calculation of the mechanical behavior of
a "honeycomb" structure (source: EC2
Modélisation/www.ec2-modelisation.fr)

Figure 2.19. Numerical simulation for composites:
manufacturing processes and mechanical properties



(a) T-joint



(b) Hull panel

Figure 2.22. Numerical simulation of welding (source: Naval Group)

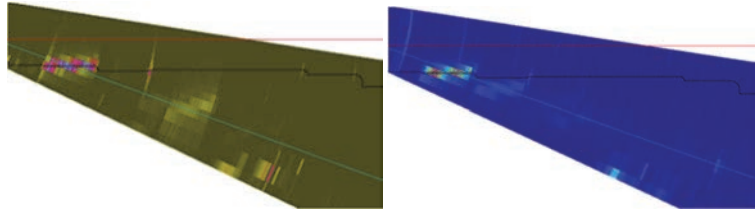
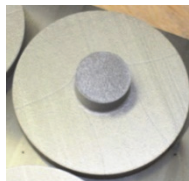
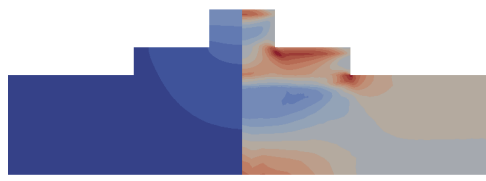


Figure 2.24. Simulation of the control of a shaft by multielement ultrasound (left) and comparison with the experiment (right) [DUP 14]



(a) Test specimen



(b) Calculation of temperature (left) and stresses (right) in the specimen

Figure 2.27. Thermomechanical numerical simulation of an additive manufacturing process on a specimen (source: ©ArianeGroup)

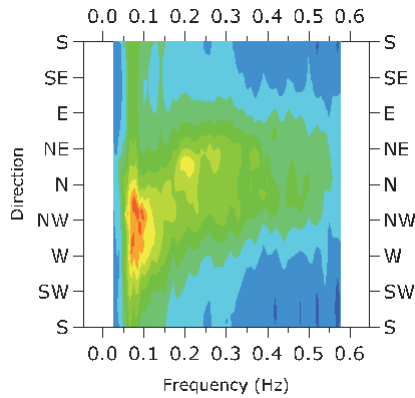


(a) LSPH collector of the “Vinci” engine

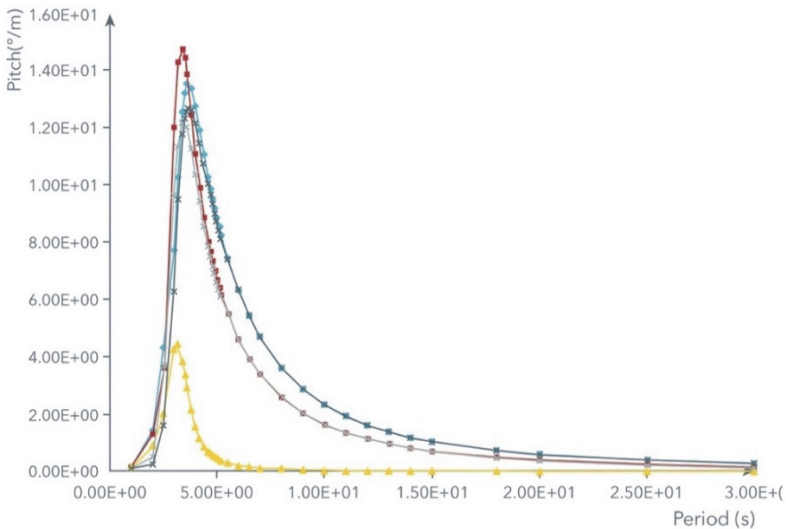


(b) Prediction of shape obtained by additive manufacturing with numerical simulation

Figure 2.28. Additive manufacturing of a real part: numerical simulation with the “inherent deformations” method (source: ©ArianeGroup)

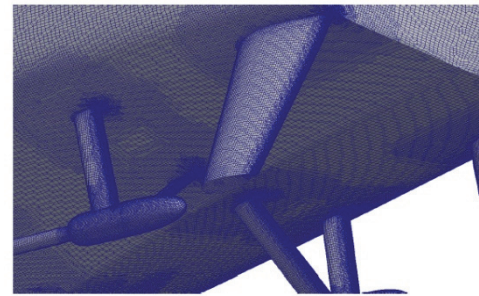


(a) Wave spectrum

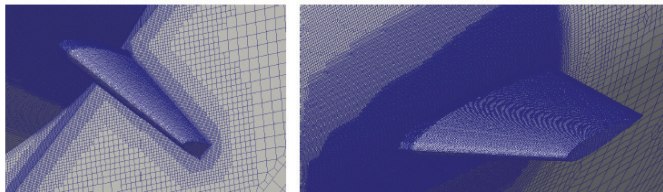


(b) Pitch movement of the vessel

Figure 2.30. Analysis of sea-keeping (source: Sirehna/Naval Group)



(a) Stern and fins



(b) Front and bottom view

Figure 2.31. Numerical model of a ship with stabilizer fins [YVI 14]

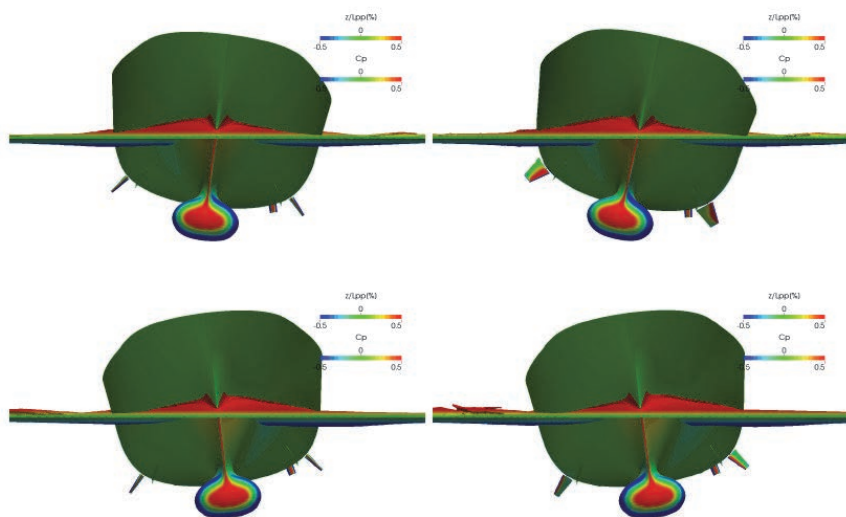


Figure 2.32. Simulation of wave resistance [YVI 14]

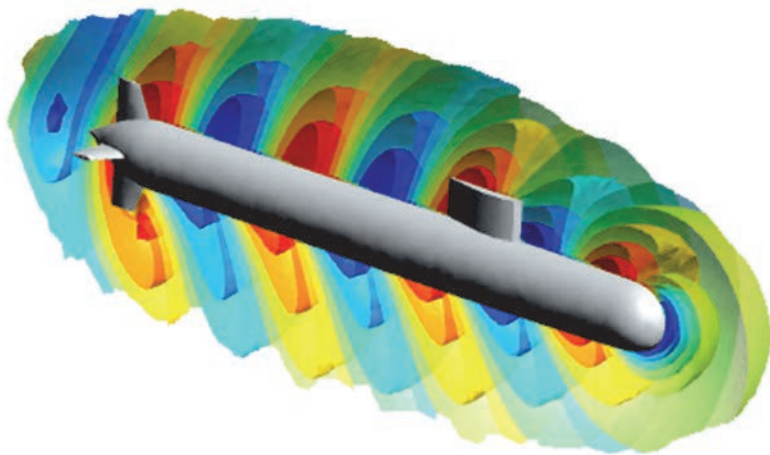


Figure 2.33. Numerical simulation of ship vibrations: example of acoustic radiation from a submarine [ANT 12]

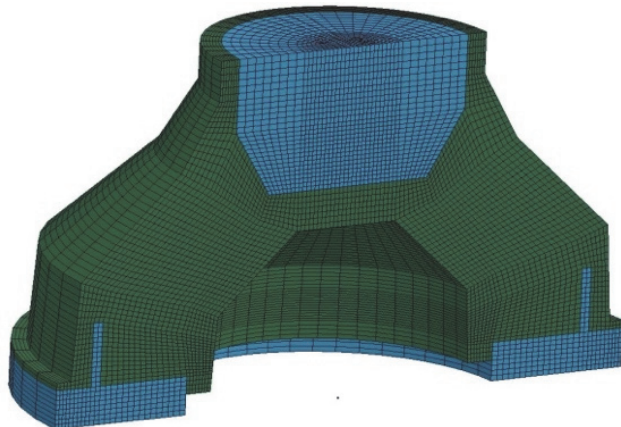


Figure 2.34. Numerical model of a suspension mount [PET 12]

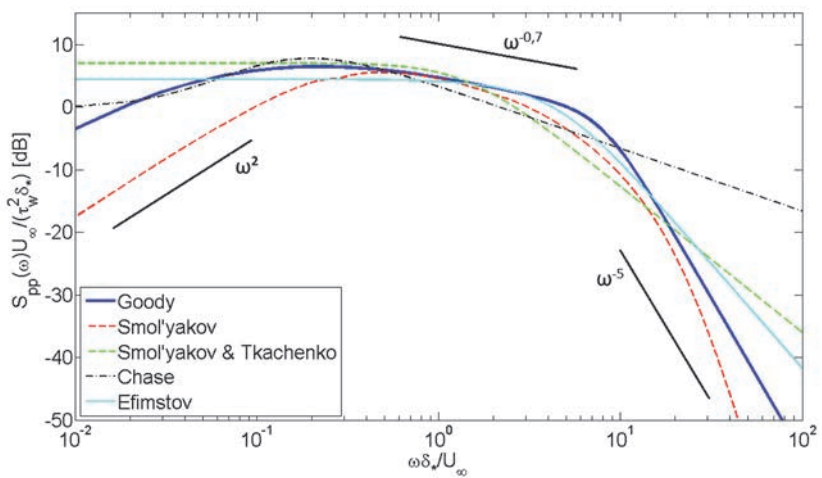


Figure 2.36. Empirical spectra of turbulent excitation [BER 14]

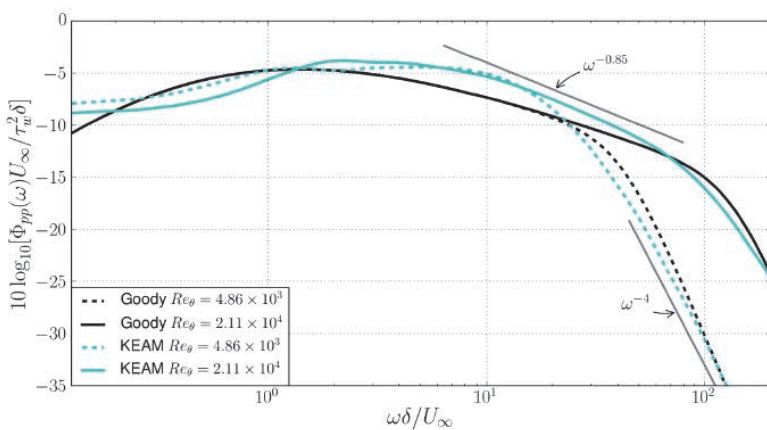


Figure 2.37. Numerically calculated and empirically determined turbulent excitation spectrum [SLA 17]



Figure 2.39. Flow simulation on an aircraft using the Lattice-Boltzmann method (source: ©Airbus)

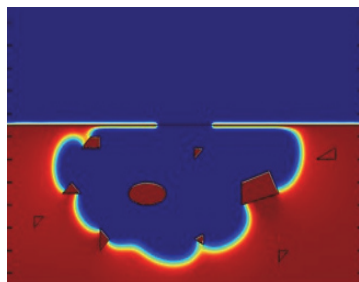


Figure 2.40. Simulation helps to understand the evolution of corrosion

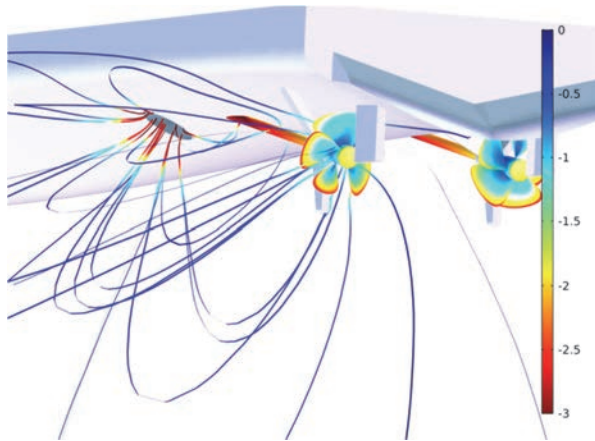


Figure 2.41. Modeling of a corrosion protection system for a ship's hull (source: image produced with the COMSOL Multiphysics® code and provided by COMSOL/ www.comsol.fr)

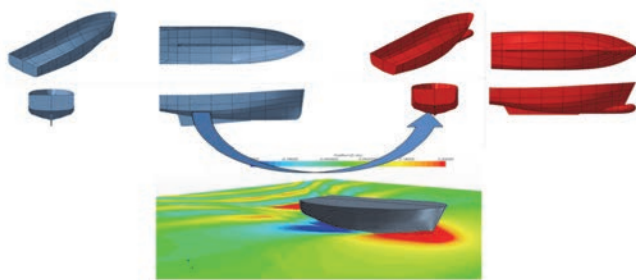


Figure 2.42. Optimization of hull shape (source: ©Sirehna/Naval Group)

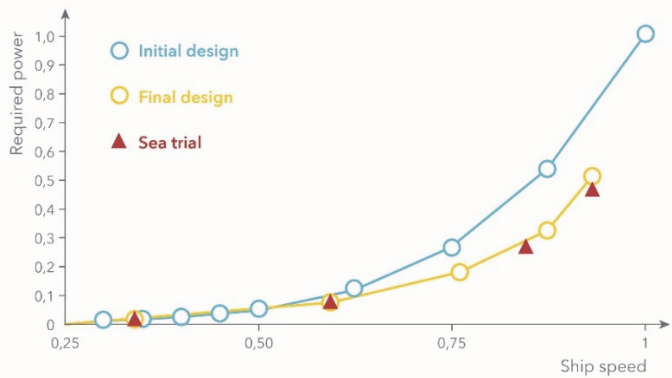


Figure 2.43. Comparison of hull performance for different ship speeds (source: Sirehna/Naval Group)

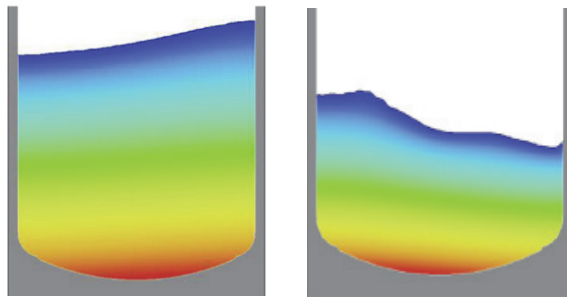


Figure 2.46. Movement of a fluid in a cryogenic reservoir [KON 19]

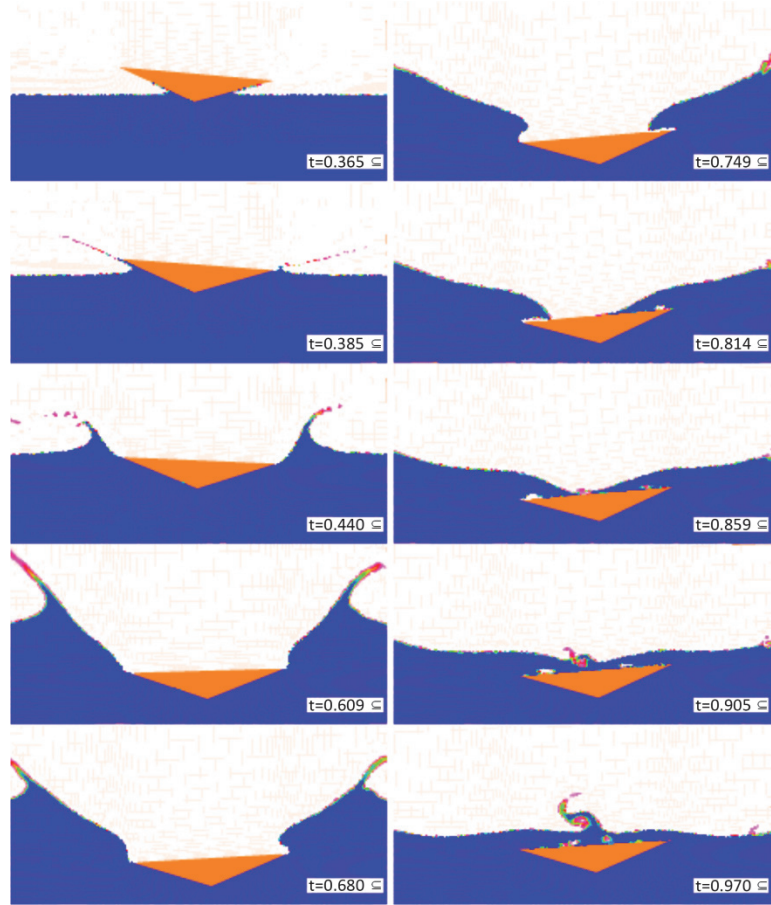


Figure 2.47. Simulation of the impact of an object on a fluid surface [LER 04]

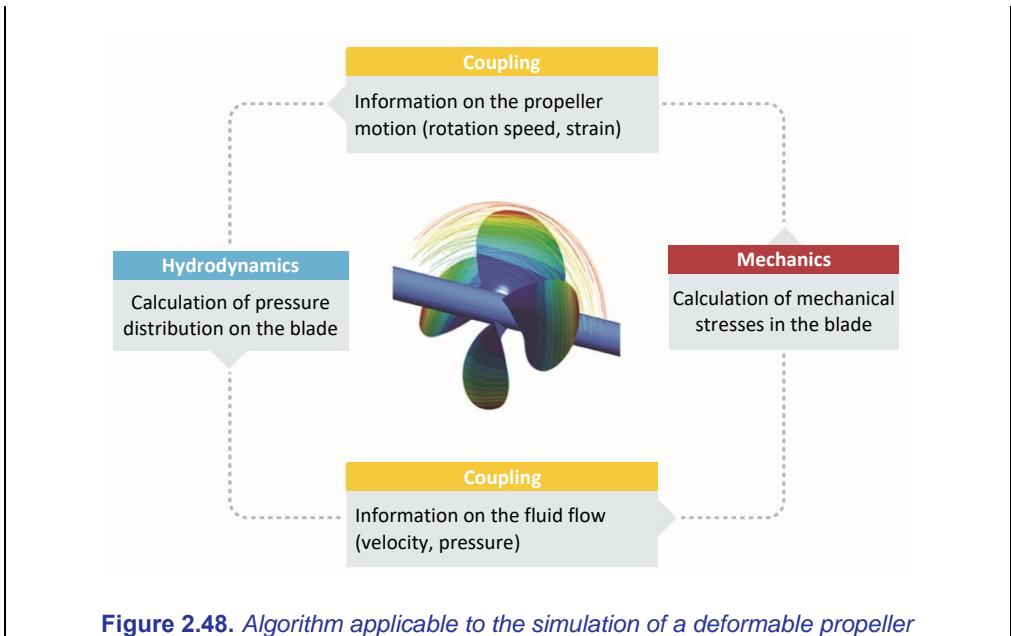


Figure 2.48. Algorithm applicable to the simulation of a deformable propeller

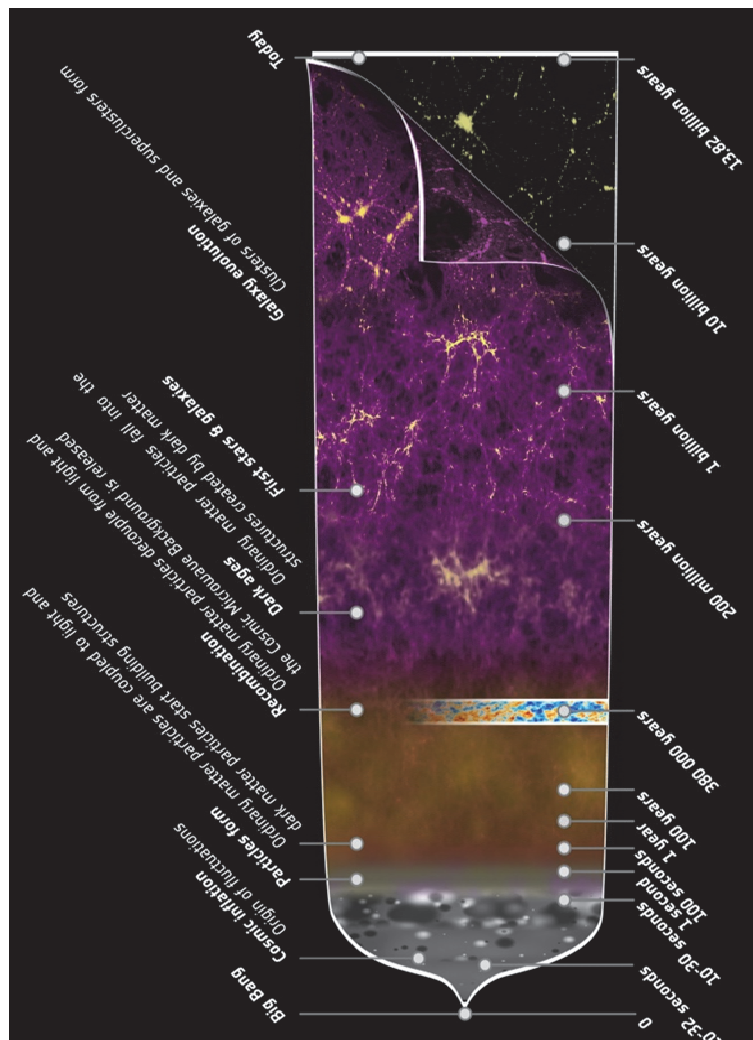


Figure 3.3. A summarizing history of the Universe

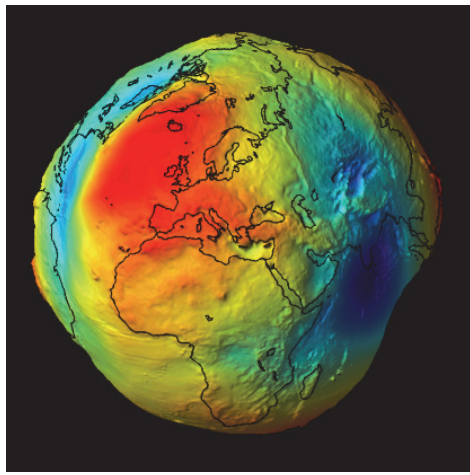


Figure 3.8. Geoid: representation of the equipotentials of the gravitational field at the Earth's surface

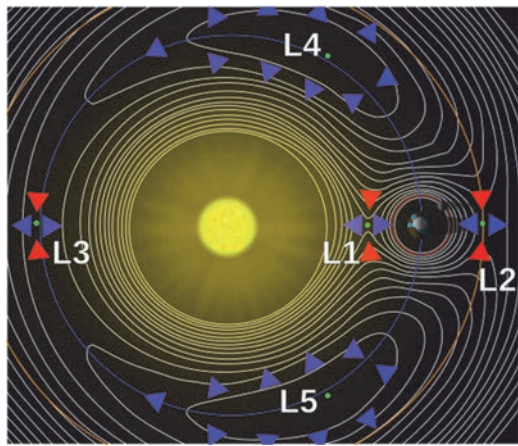


Figure 3.9. Lagrange points for the Sun and Earth



Figure 3.10. The Interplanetary Transport Network (ITN) passes through the Lagrange points of different planets of the solar system (source: ©NASA)

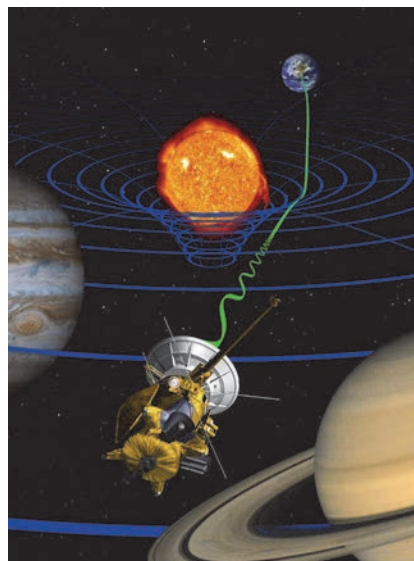


Figure 3.11. Signals sent between the Earth and the Cassini probe (green wave) are delayed by the deformation of space and time due to the mass of the Sun (source: ©NASA)

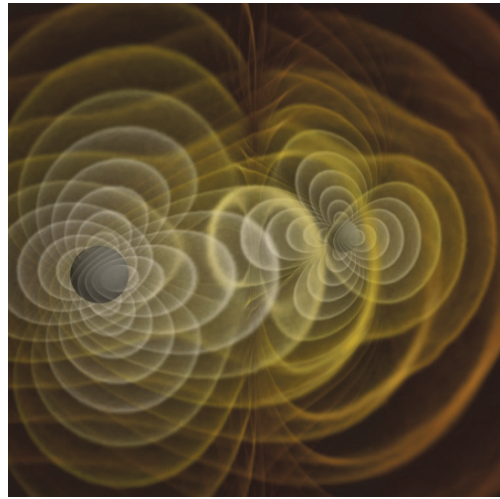


Figure 3.12. Simulation of gravitational waves resulting from the interaction between two massive celestial bodies

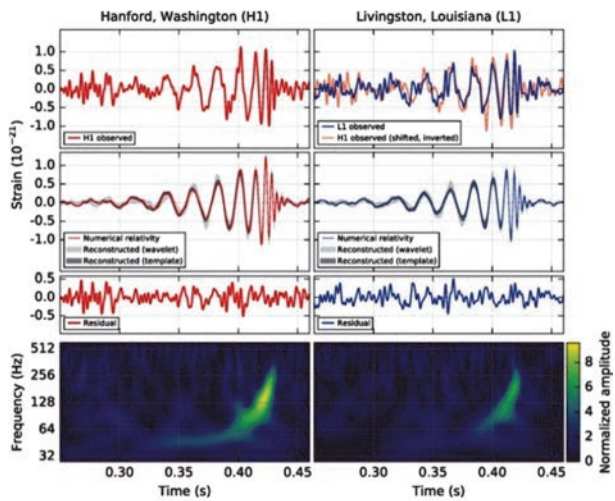


Figure 3.14. First detection of gravitational waves, named after the day of their discovery, September 15, 2014: GW150914 [ABO 16]

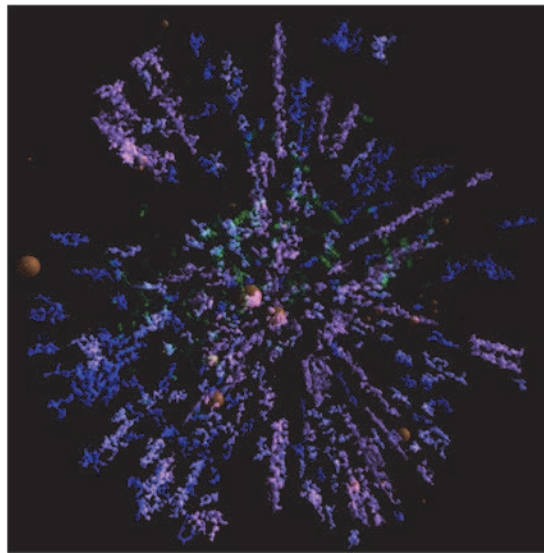


Figure 3.17. Stellar density map of our galaxy

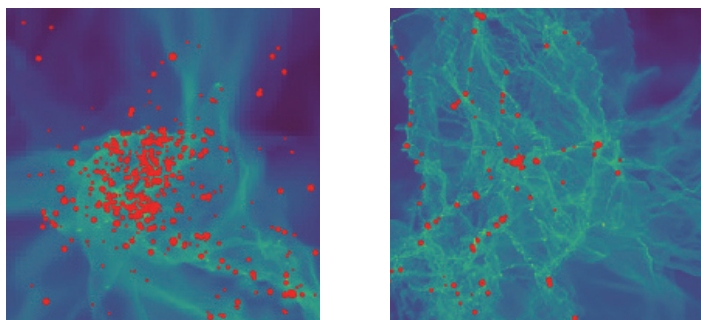


Figure 3.18. Stellar density calculations in a star cloud [LEE 17a]

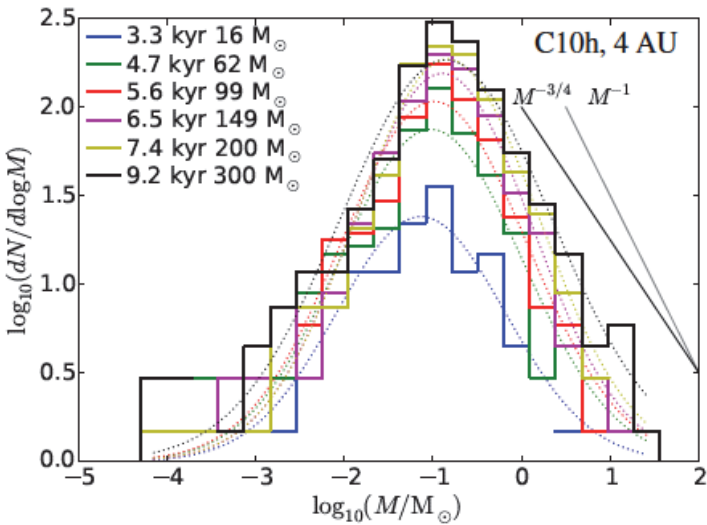


Figure 3.19. Stellar density calculations [LEE 17b]

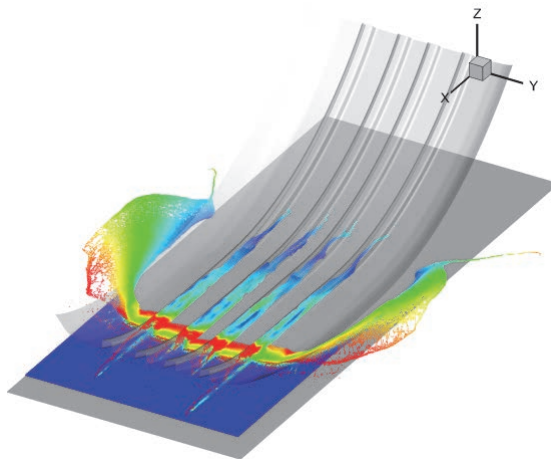


Figure 3.20. Aquaplaning simulation [HEM 17]

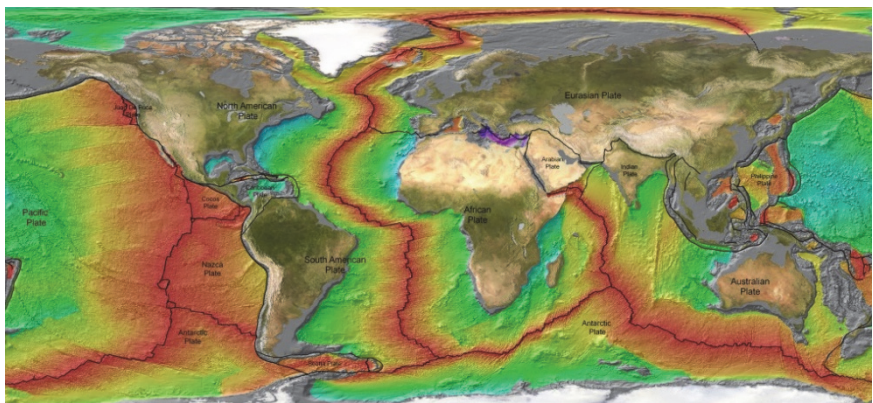


Figure 3.22. Age of the oceanic lithosphere [MUL 11]

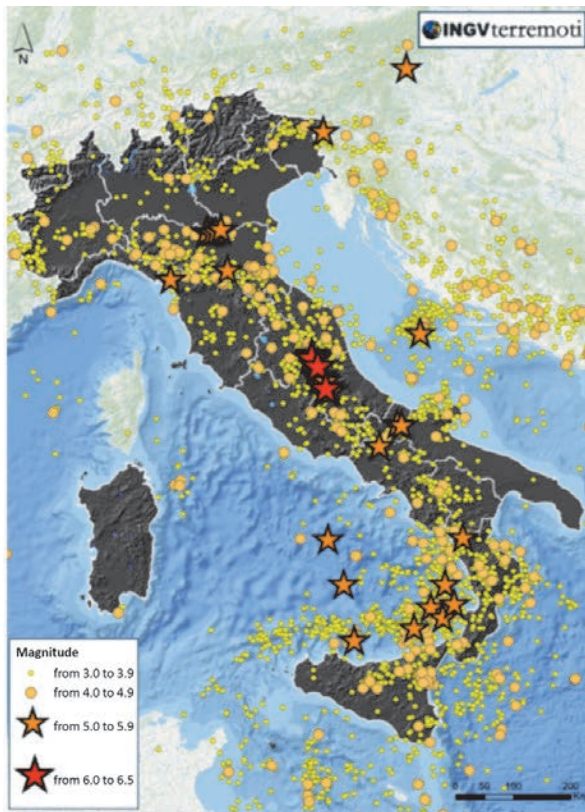


Figure 3.23. Recent seismic history of Italy (source: Emanuele Casarotti, National Institute of Geophysics and Volcanology)

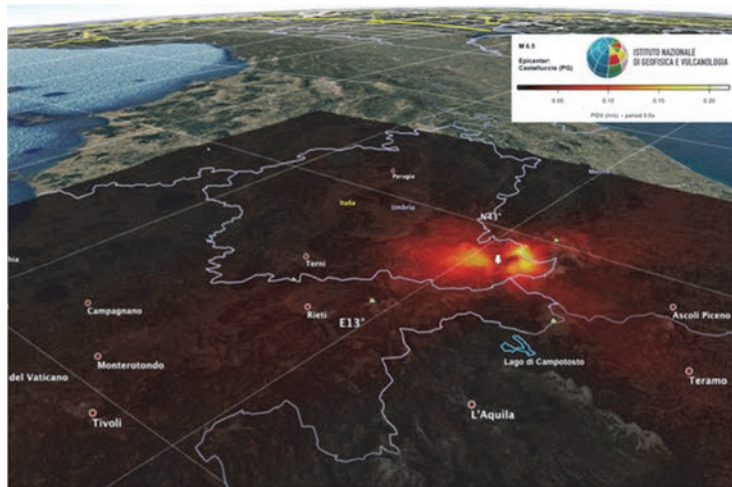


Figure 3.24. Scenario for the L'Aquila earthquake aftershock: in yellow and red, the areas potentially affected (source: calculations were carried out in 2009 by Dimitri Komatitsch at the Centre National de la Recherche Scientifique in France and Emanuele Casarotti at the National Institute of Geophysics and Volcanology in Italy)

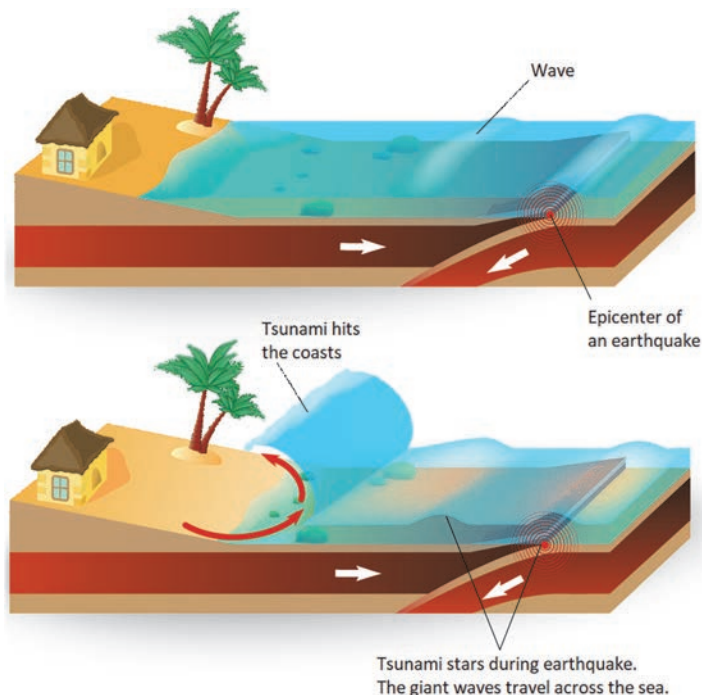


Figure 3.26. An underwater earthquake can cause a tsunami (source: © www.shutterstock.com)

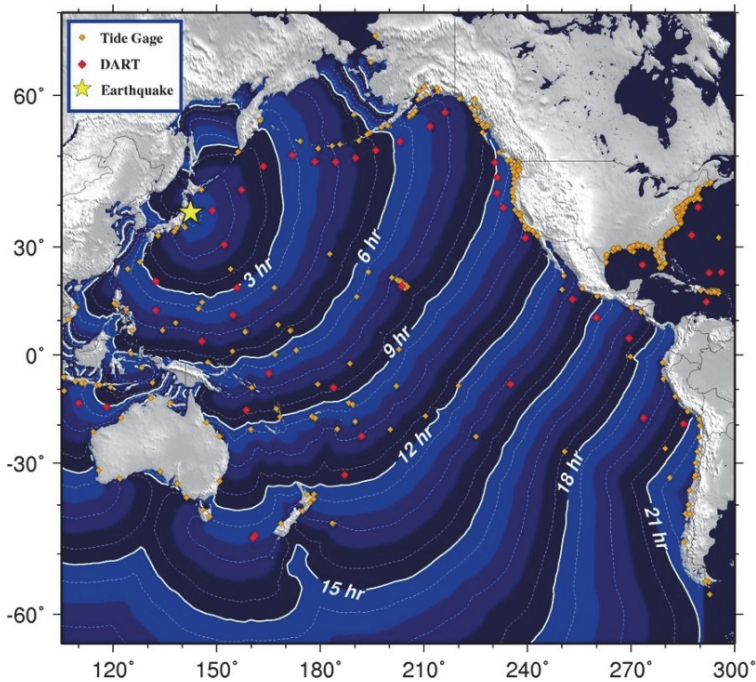


Figure 3.27. Estimated time for tsunami wave velocity induced by the Sendai earthquake in 2011 according to the National Oceanic and Atmospheric Administration (source: ©NOAA/www.noaa.gov)

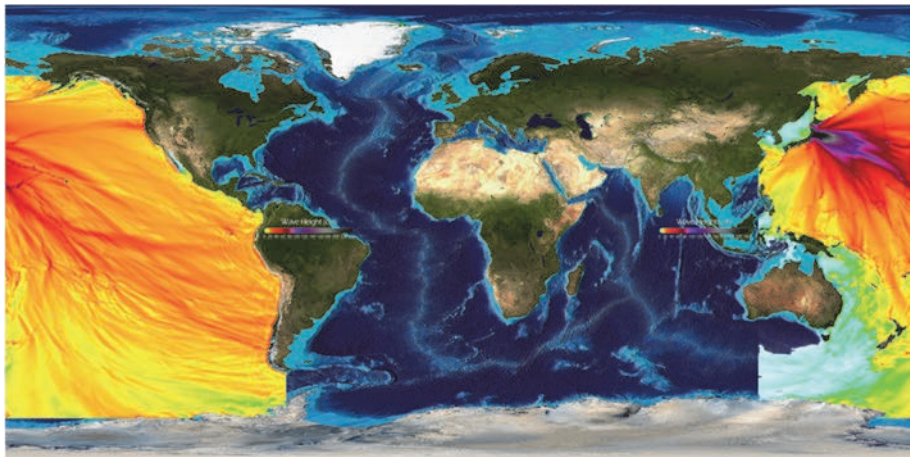


Figure 3.28. Tsunami wave height induced by the Sendai earthquake in 2011 estimated by the National Oceanic and Atmospheric Administration (source: ©NOAA/www.noaa.gov)

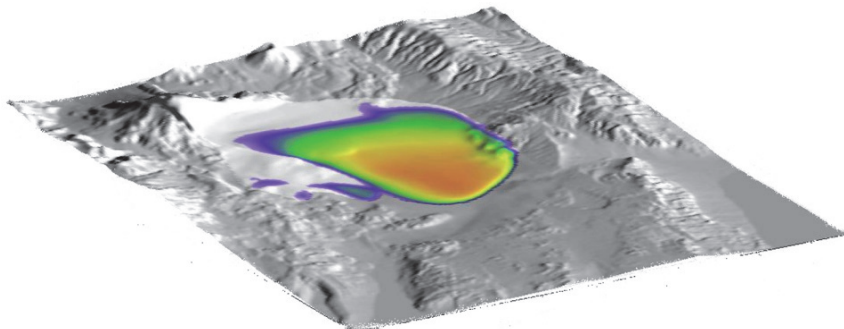


Figure 3.31. Simulation of an avalanche of volcanic debris [KEL 05]

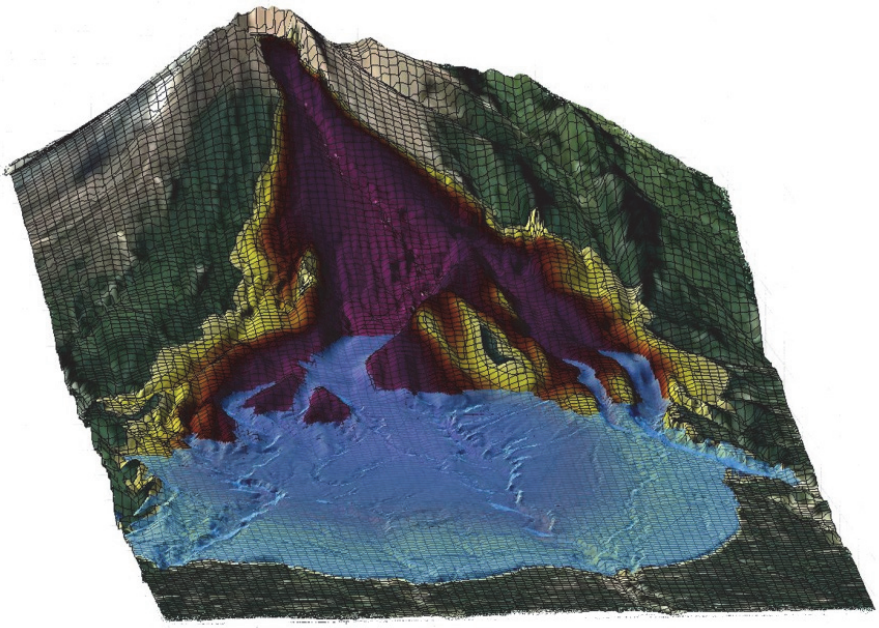


Figure 3.34. Simulation of the 2010 eruption of the Merapi volcano in Indonesia with the VolcFlow code [KEL 17b]

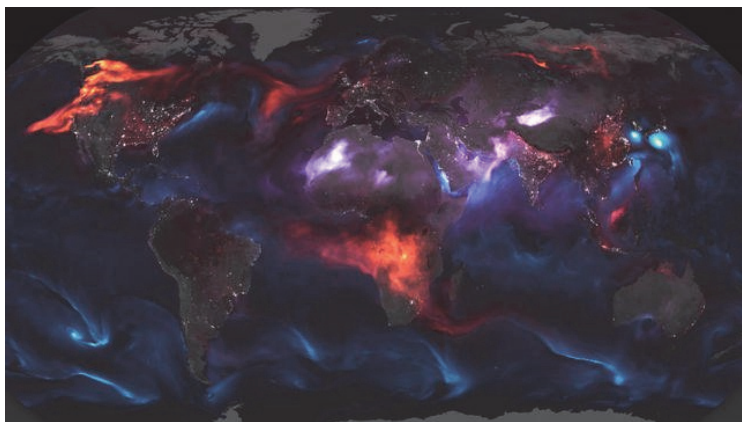


Figure 4.2. Emissions of substances into the Earth's atmosphere (source: © NASA/J. Stevens and A. Voiland)

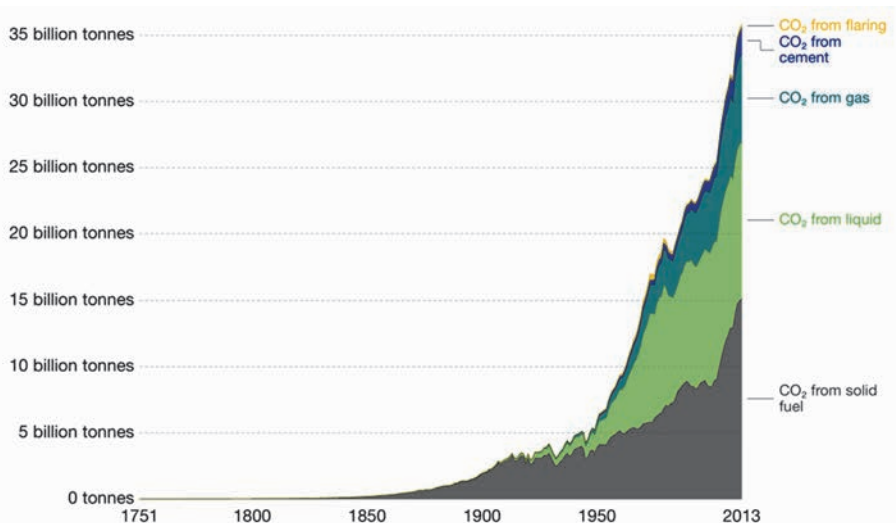


Figure 4.3. CO₂ emissions from different sources (source: Our World in Data/<https://ourworldindata.org/co2-and-other-greenhouse-gas-emissions>)

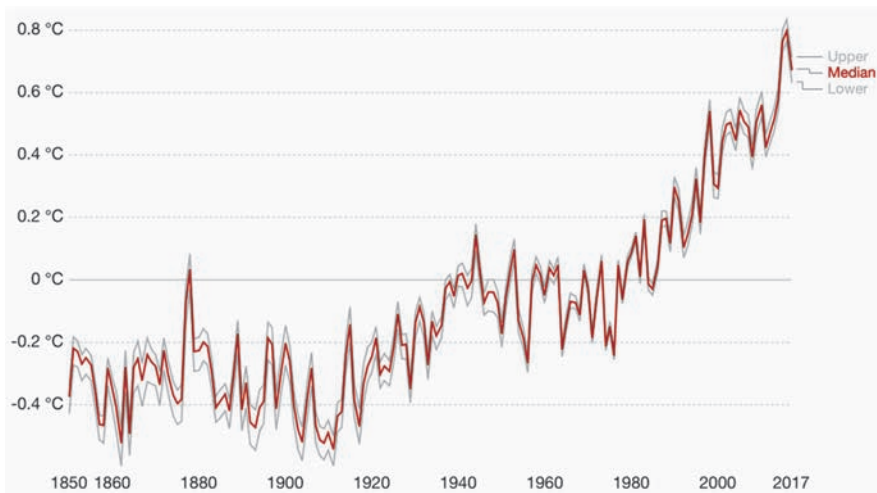


Figure 4.4. Evolution of the average temperature at the Earth's surface from 1850 to 2017
(source: Our World in Data/<https://ourworldindata.org/co2-and-other-greenhouse-gas-emissions>)

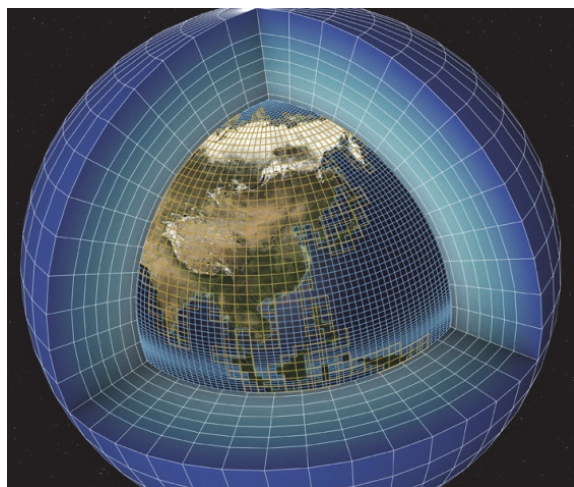


Figure 4.5. Meshing of the atmosphere (source: © ISPL/CEA-DSM)

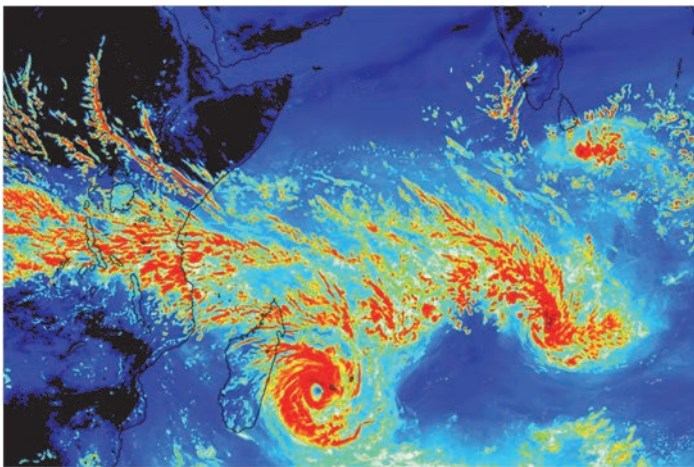


Figure 4.6. Numerical simulation of a cyclone off the island of Madagascar (source: ©CERFACS)

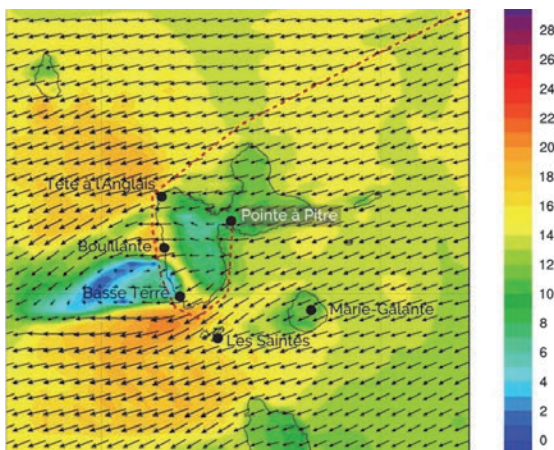


Figure 4.7. Simulation of wind conditions around: the wind scale is indicated in knots (source: www.metigate.com)

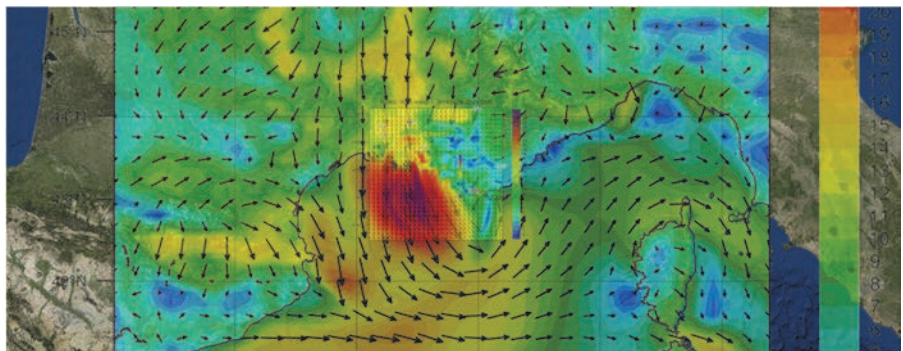


Figure 4.8. Downscaling principle: local simulation on the Marseille region based on global data on the South-East of France (source: www.metigate.com)

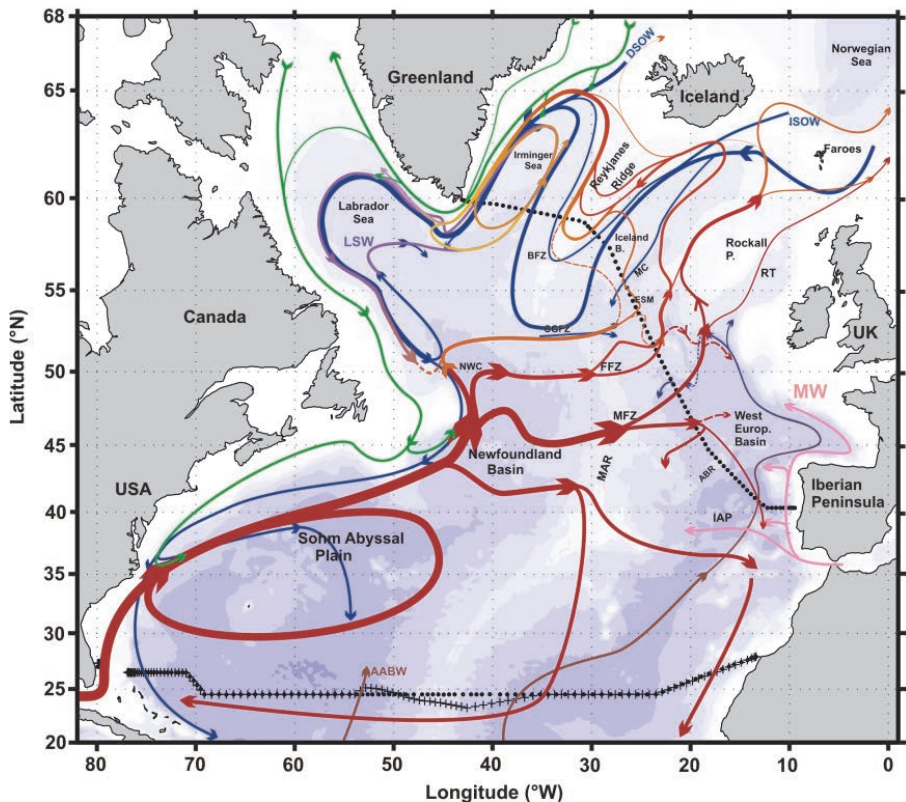


Figure 4.9. The main currents of the North Atlantic (source: © IFREMER)

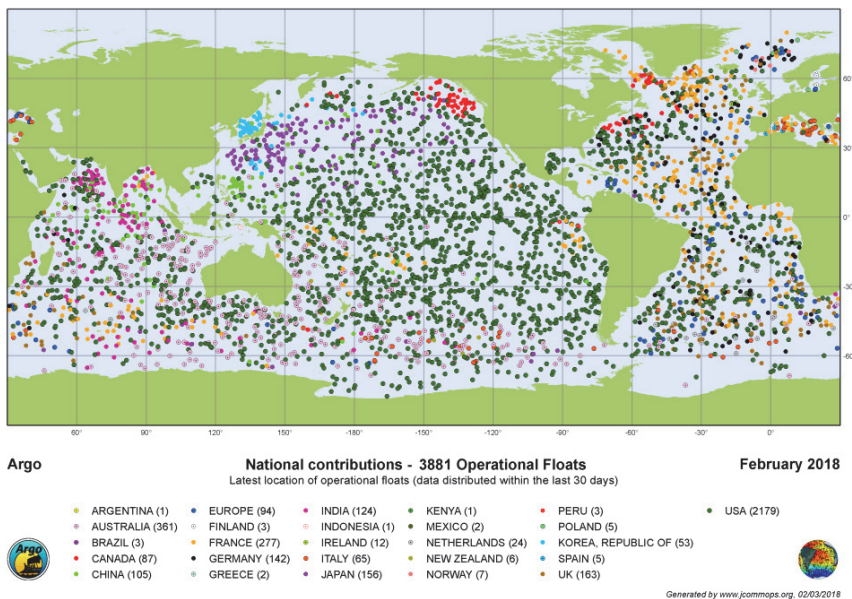


Figure 4.11. The international program “Argo” collects oceanological data through a network of nearly 4,000 floats spread throughout the world’s seas and oceans (source: www.commons.wikimedia.org)

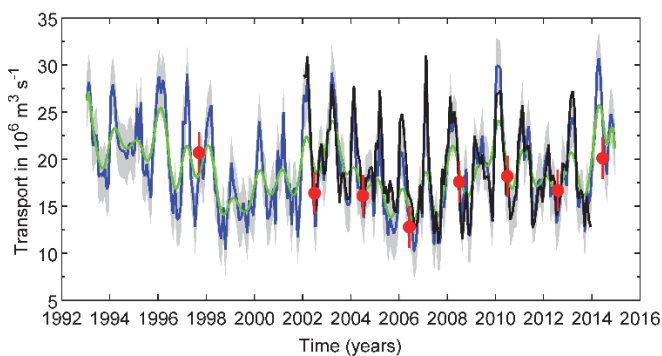


Figure 4.12. Evolution of ocean transport relative to the North Atlantic “conveyor belt” between 1992 and 2016 (source: © IFREMER/CNRS/UBO)

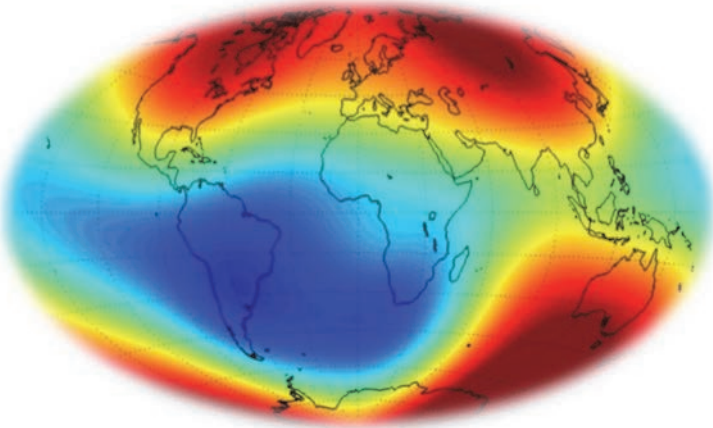


Figure 4.13. The Earth's magnetic field measured from space (source: © ESA/ www.esa.int)

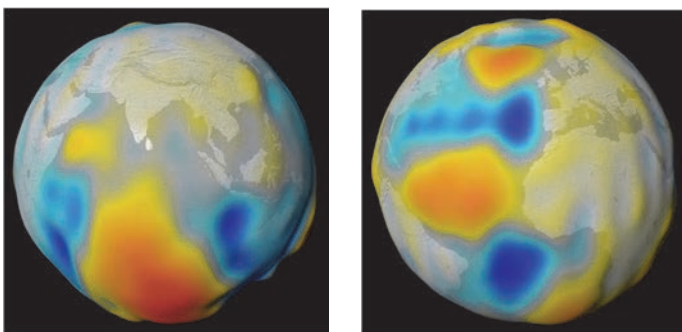


Figure 4.14. Images of the magnetic field generated by ocean currents (source: https://www.esa.int/spaceinvideos/Videos/2018/04/Magnetic_tides)

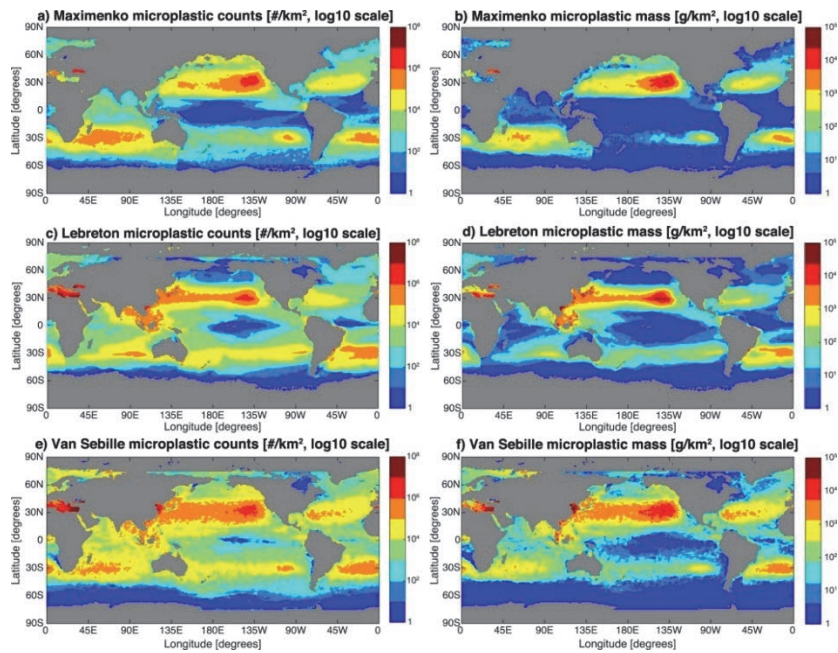
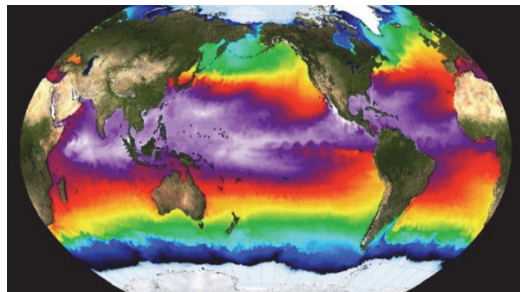
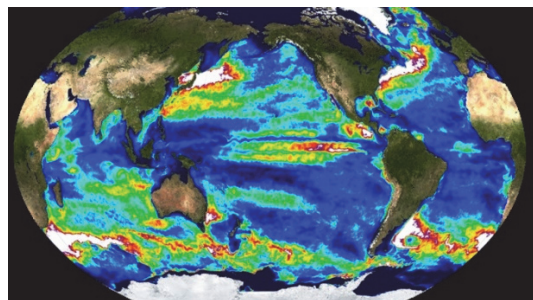


Figure 4.16. Estimated number and mass of plastic microparticles in the oceans [SEB 15]



(a) Mean temperature



(b) Temperature variability

Figure 4.20. Calculation of ocean surface temperature

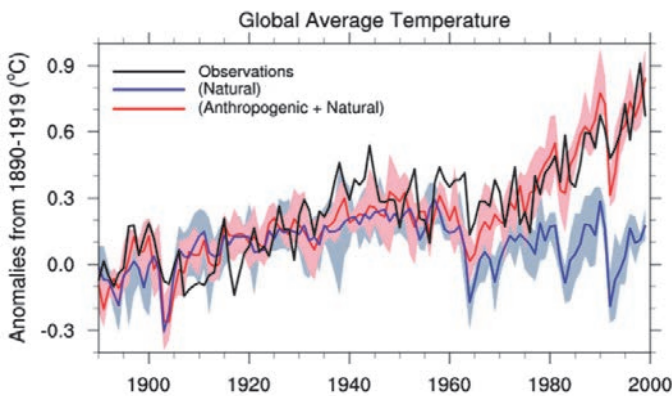


Figure 4.21. Contributing to the study of climate, numerical modeling is used to understand the influence of human activities on the global temperature evolution observed in the 20th Century [MEE 04]

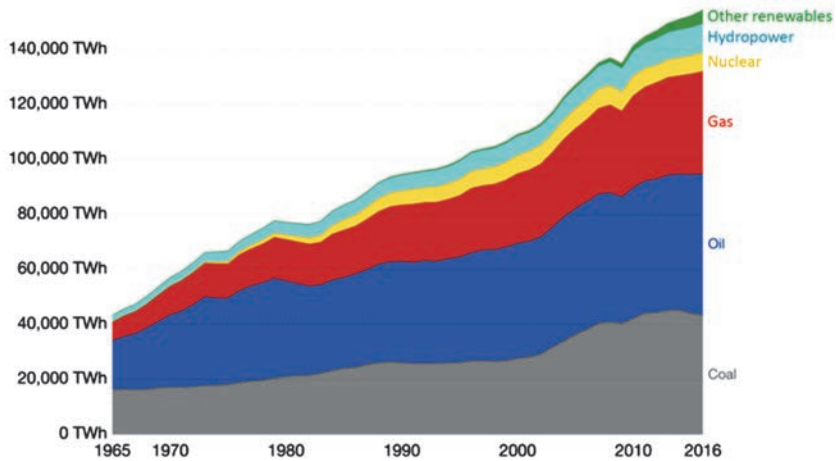


Figure 5.2. Evolution of world energy consumption between 1965 and 2016 (source: Our World in Data/ <https://ourworldindata.org/energy-production-and-changing-energy-sources>)

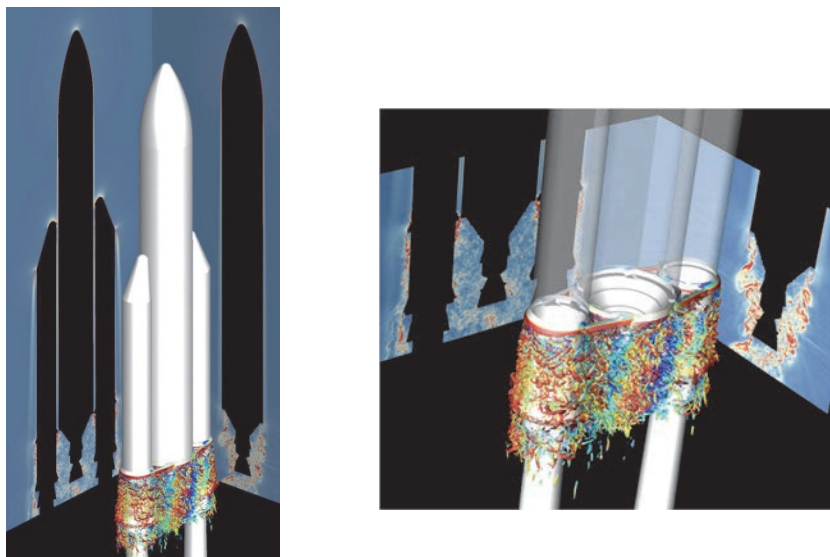


Figure 5.3. Back body calculation for Ariane V (source: ©ONERA)



Figure 5.5. Simulation of a gas turbine ignition sequence [BOI 08]

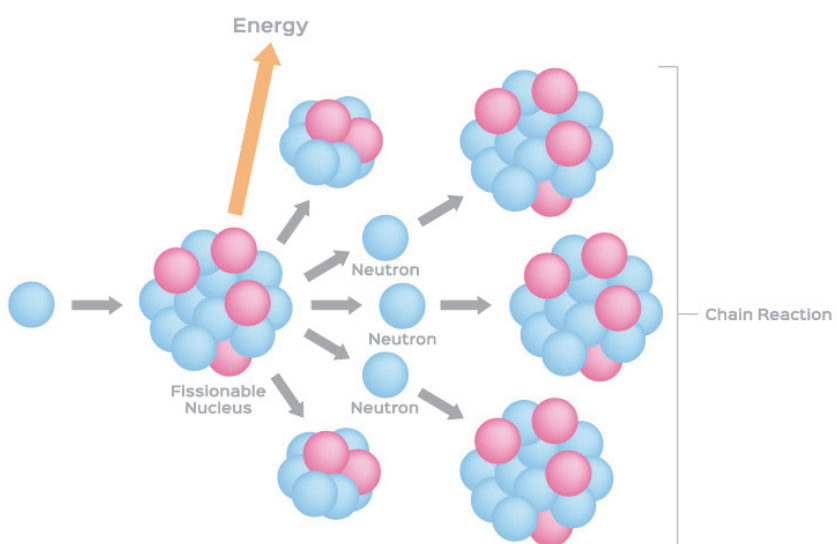


Figure 5.8. Nuclear fission (source: www.shutterstock.com)

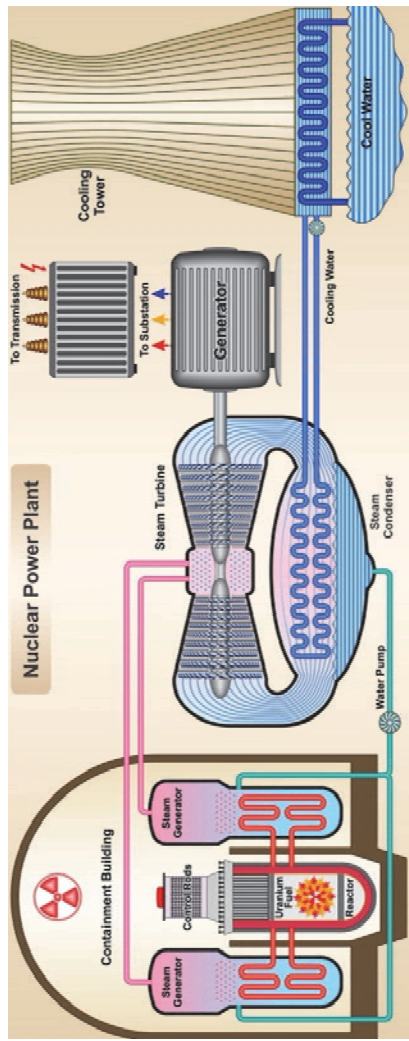


Figure 5.9. Schematic diagram of the operation of a nuclear power plant (source: www.123rf.com/Fouad Saad)

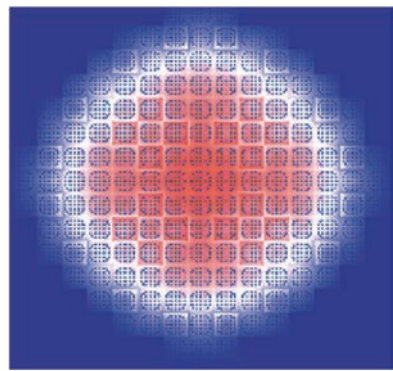


Figure 5.10. Power map of a pressurized water reactor [CAL 11]

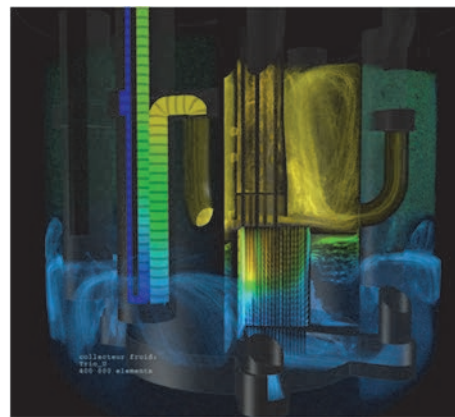


Figure 5.11. Multiscale thermo-hydraulic calculations of a 4th generation reactor core (source: calculation performed with the CATHARE system code, the Trio-MC core code and the TrioCFD CFD code – ©CEA/Direction de l'Énergie Nucléaire)

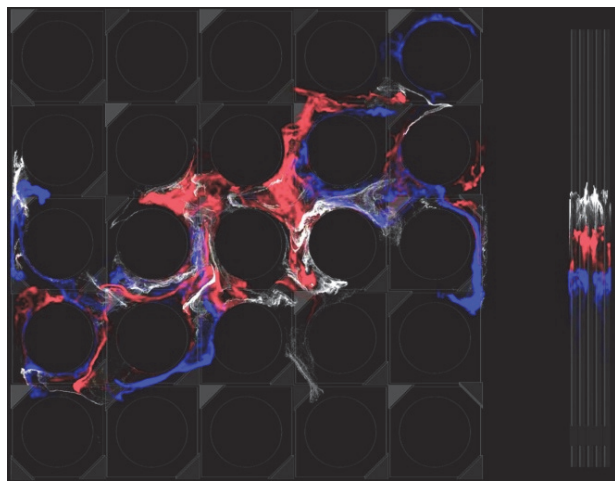


Figure 5.12. Calculation of the LES in an reactor mixing grid (source: Christophe Calvin/Commissariat à l'Énergie Atomique)

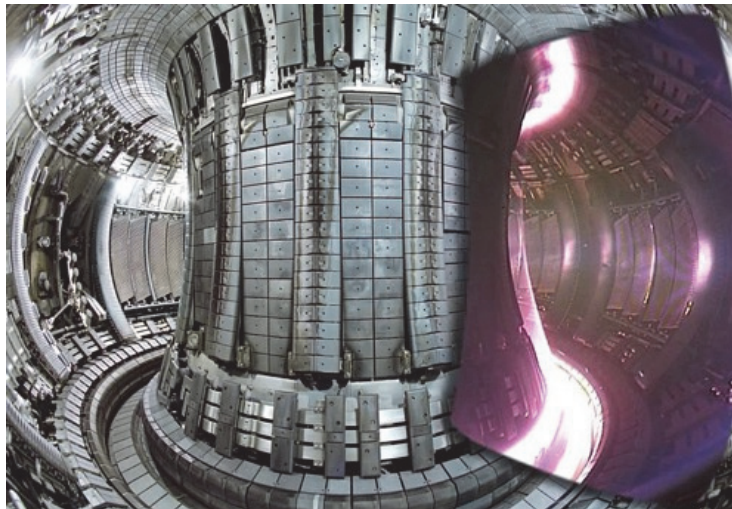


Figure 5.14. Obtaining a plasma in a device: example of the European JET “tokamak” before and during its operation (source: www.iter.org)

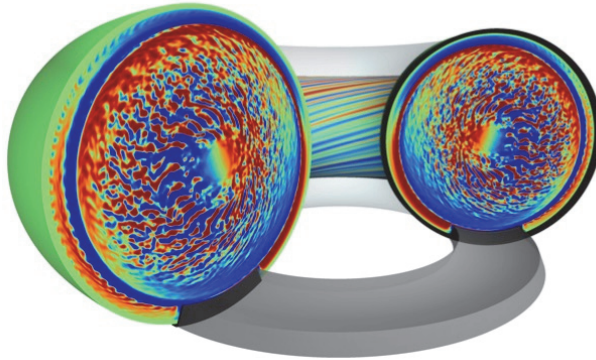


Figure 5.15. Simulation of turbulence developing in a tokamak

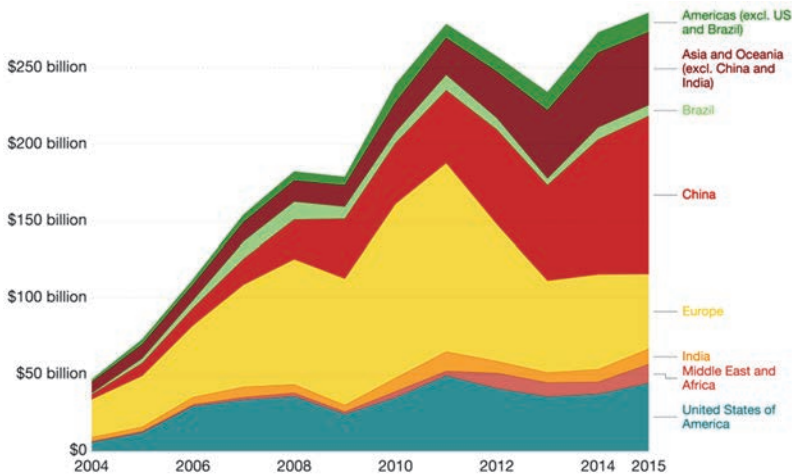
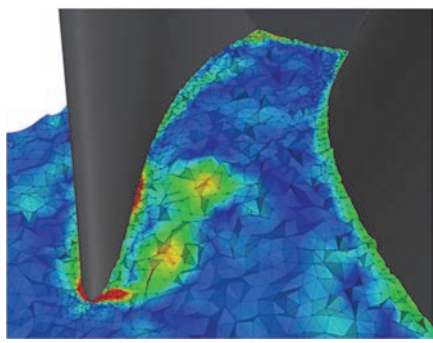
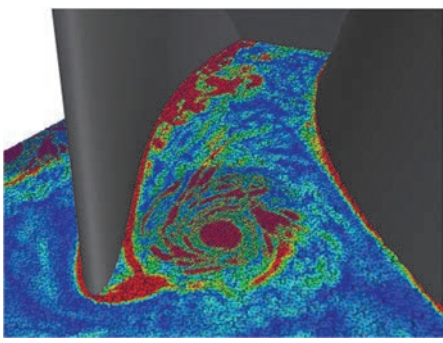


Figure 5.16. Global investment in renewable energy (source: Our World in Data/<https://ourworldindata.org/renewables>)



(a) 4 million cells

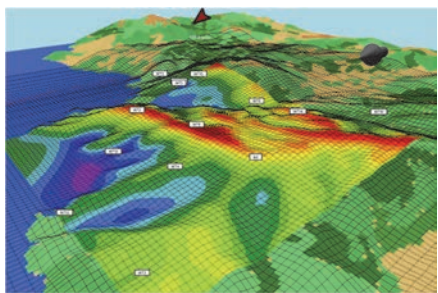


(a) 80 million cells

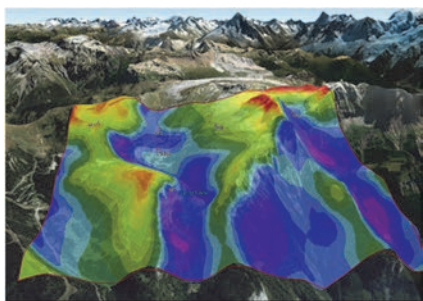
Figure 5.19. Mesh size used for LES simulation of a turbine body [DOU 18]



Figure 5.21. Flow calculation around a vertical axis wind turbine
(source: Institut P' <https://www.pprime.fr/>)



(a) Numerical calculation model



(b) Projection of results on site

Figure 5.23. Evaluation of a site's wind resource (source: calculation carried out with the MeteoDyn/WT6 software by the company MeteoDyn/www.meteodyn.com)

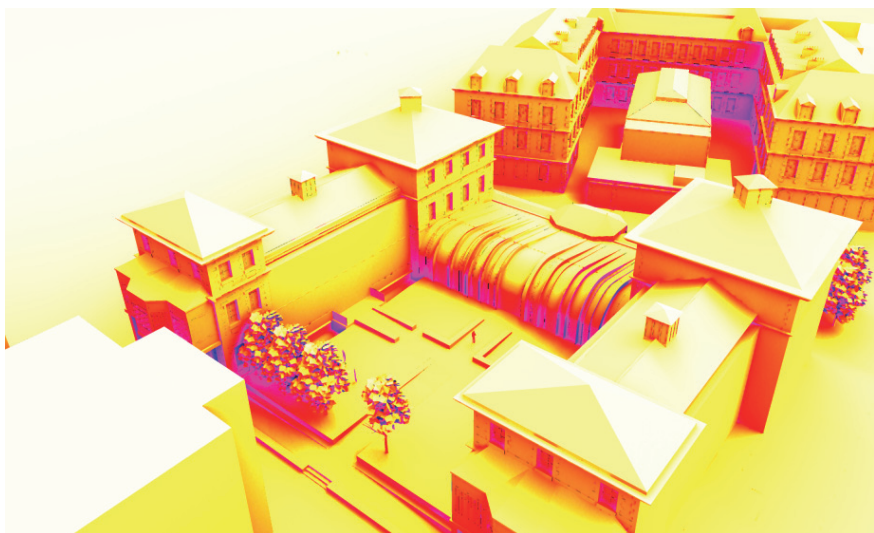
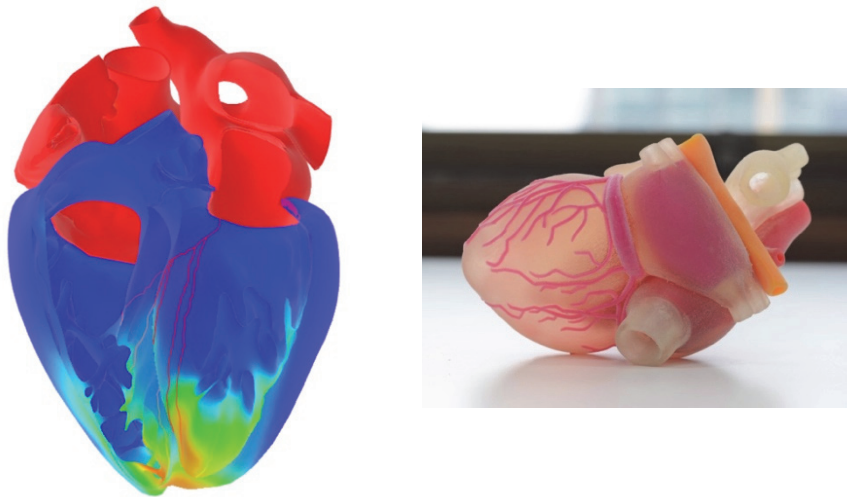


Figure 5.24. Evaluation of the effects of sunlight on an urban area using dynamic thermal simulations (source: www.inex.fr)



(a) "The Living Heart Project" develops the digital simulation of a heart [BAI 14] (source: Dassault Systèmes)

(b) Heart model obtained by 3D printing (source: www.shutterstock.com)

Figure 6.2. "In silico" model and new generation "in vitro" model

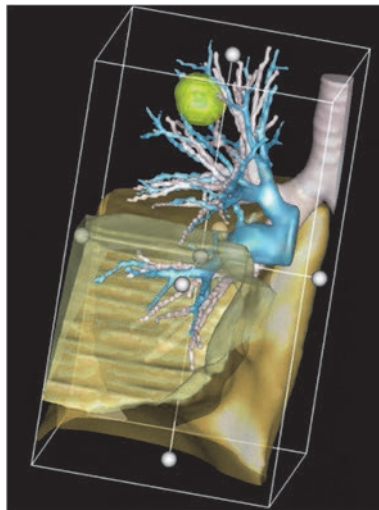


Figure 6.3. The area to be operated on, in this case a tumor, is identified on a patient's digital medical imaging file (source: Jean-Marc Baste, Rouen University Hospital)



Figure 6.7. Identification of the main fiber bundles of the brain based on diffusion MRI (source: Jean-François Mangin, Vincent El Kouby, Muriel Perrin, Yann Cointepas, Cyrille Poupon/Commissariat à l'Énergie Atomique, NeuroSpin center)

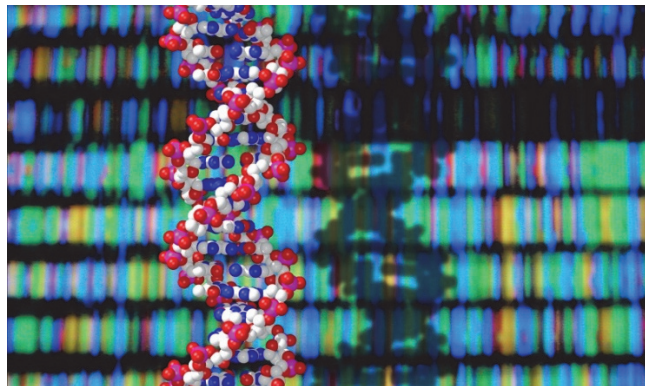


Figure 6.10. Sequencing techniques allow scientists to decode the human genome from the molecular structure of the DNA



Figure 6.11. Finite element model of a leg's soft tissue (source: image owned by Texisense and the TIMC-IMAG laboratory)

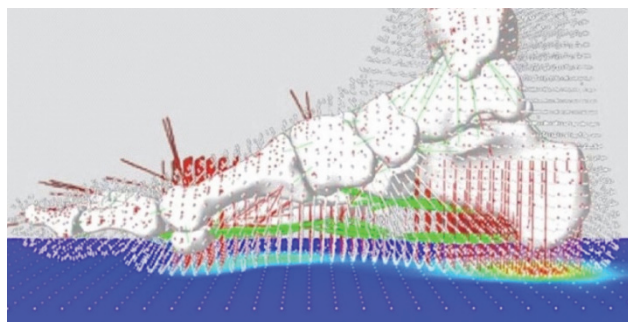
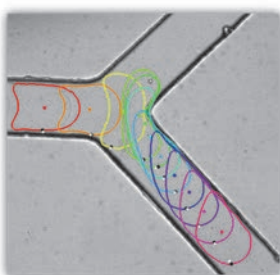
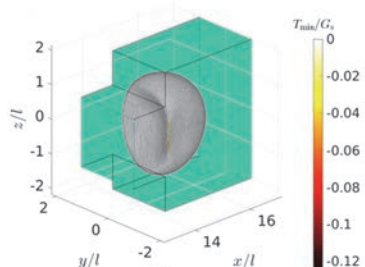


Figure 6.12. Pressure calculated in a foot under pressure on the ground (source: image owned by Texisense and the TIMC-IMAG laboratory)

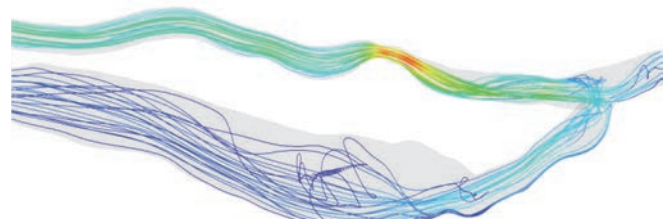


(a) Flow visualization

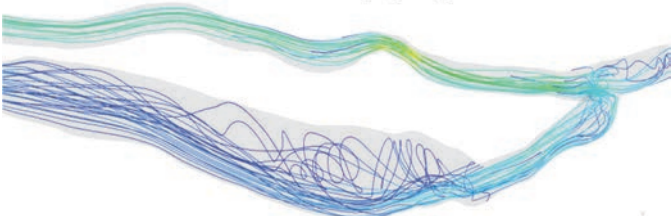


(b) Numerical simulation [SAR 18]

Figure 6.14. Flow of a microcapsule (100 large microns) into a channel of the same size with sudden widening (transition to a rectangular channel [SEV 16] or Y-shaped opening [CHU 13])



(a) Before angioplasty



(b) After angioplasty

Figure 6.18. Numerical simulation of blood flow in an arteriovenous fistula [DEC 14]



Figure 6.20. Simulation of stent placement in angioplasty: personalized arterial geometry, CAD model and finite elements and aortic prosthesis placement [PER 15]

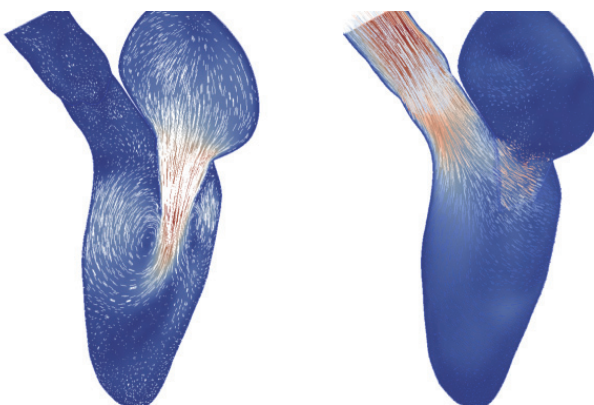


Figure 6.21. Coupled fluid/structure simulations in the heart: blood flow rate in the left ventricle (source: INRIA/ REO and M3DISIM project teams)

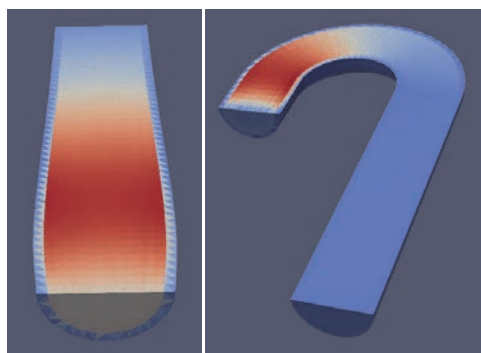


Figure 6.22. Simulations of blood flow in a right (left) and curved (right) artery using a “monolithic” algorithm [MUR 17b]

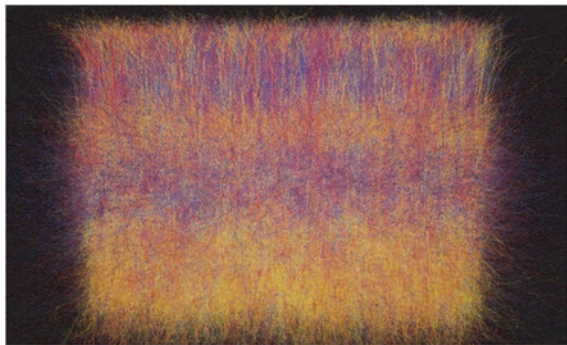


Figure 6.23. Simulation of the electrical activity of a portion of a virtual brain consisting of seven reconstructions of neocortical microcircuits (source: © The Blue Brain Project/www.bluebrain.epfl.ch)

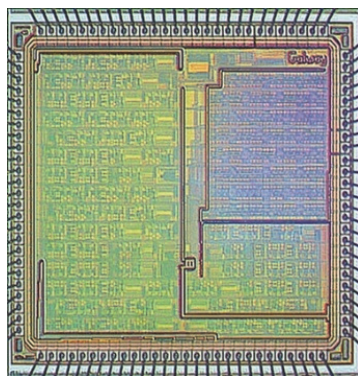


Figure 6.24. Galway neuro-morphic processor (source: Timothée Lévi, Université de Bordeaux)

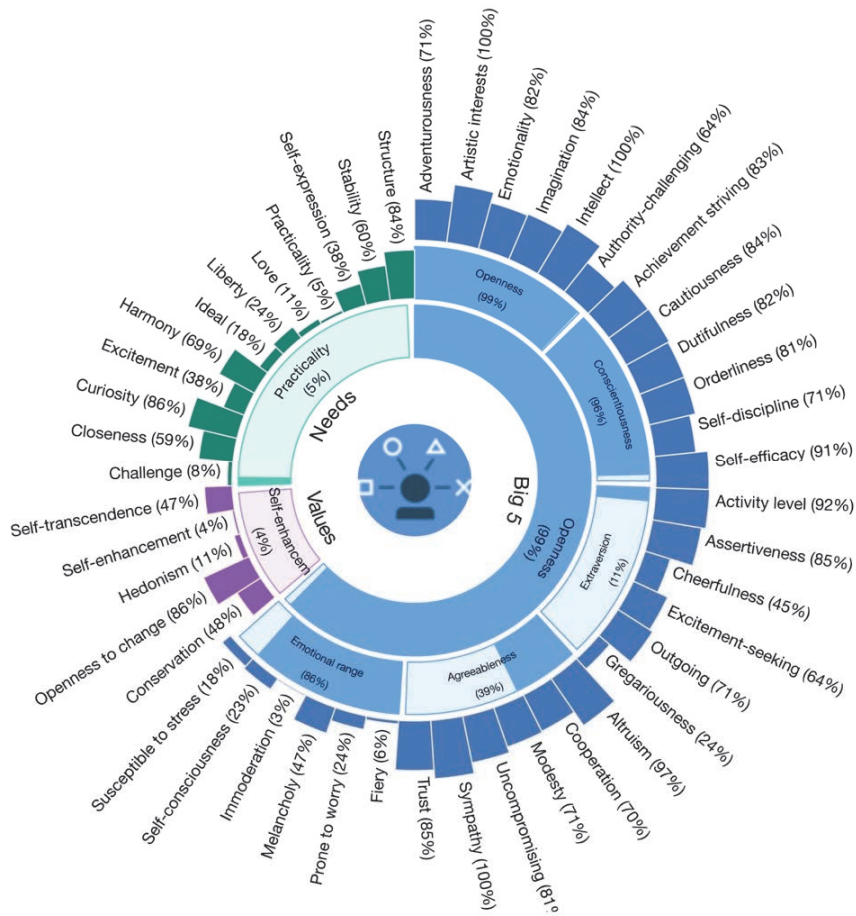


Figure 7.5. An automatic analysis of personality traits

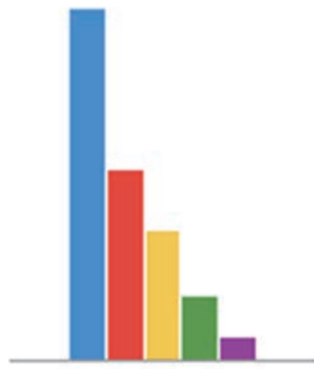


Figure 7.6. Hierarchy of keywords #Sex (blue), #Weather (red), #Love (yellow), #Food (green) and #God (purple) in Google searches from 2004 to 2018 (source: <https://trends.google.com/>)

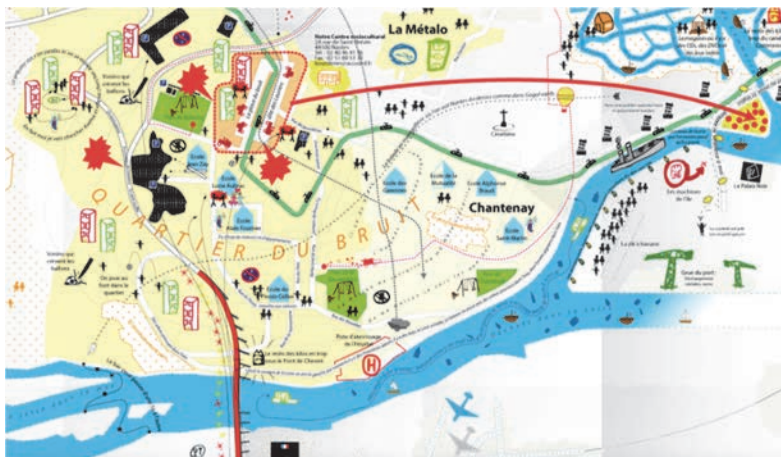


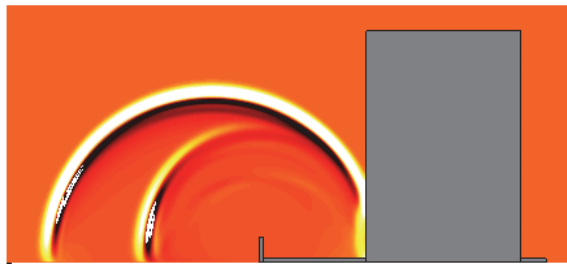
Figure 7.8. Subjective map of the city of Nantes (source: <http://www.geographiesubjective.org>)



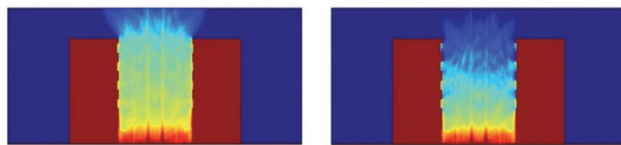
Figure 7.9. Mobility simulation in the defense district



Figure 7.10. Road noise map of the city of Nantes (source: IFSTTAR/CEREMA)



(a) Assessment of the influence of a right screen on sound propagation around a building [PIC 12]



(b) Assessment of the influence of building greenery on the noise environment of a street at 100 Hz (source: IFSTTAR)

Figure 7.11. Acoustic propagation simulations with “detailed modeling”

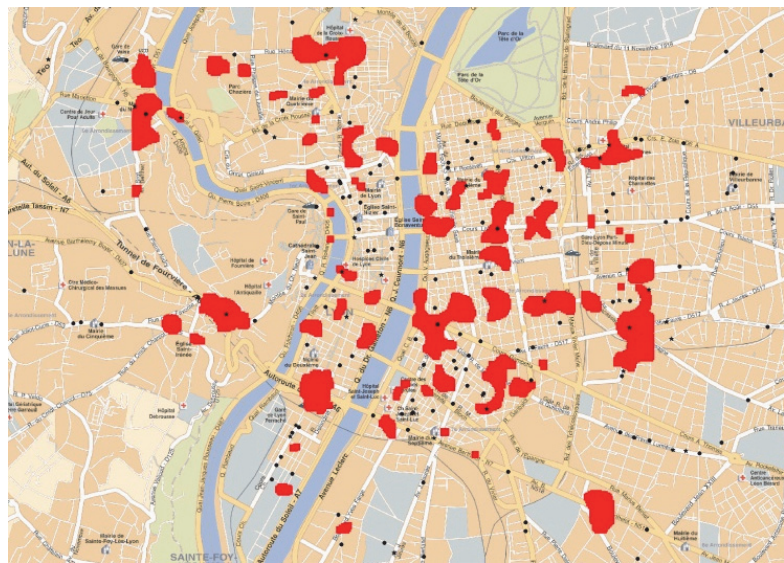


Figure 7.13. The best places to open a bakery in Lyon (source: Pablo Jensen, École Normale Supérieure de Lyon)

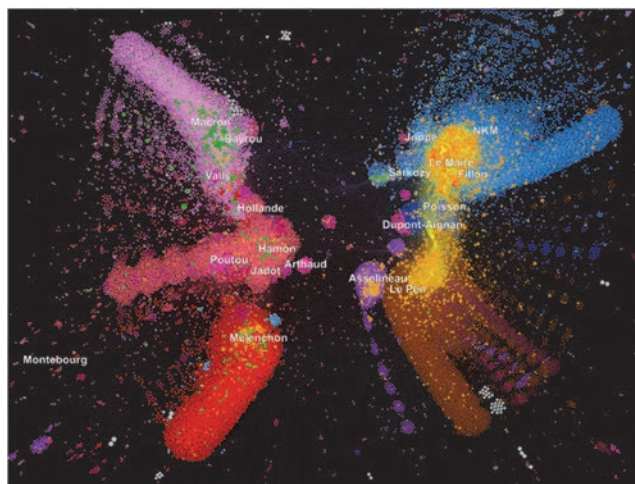


Figure 7.16. Analysis of information relayed on Twitter during the French presidential campaign in 2017 [GAU 18]